




Charged-particle emission in neutron reactions on ^{10}B

T. N. Massey ^{*}, J. E. O'Donnell, J. Ralston, S. M. Grimes , and C. R. Brune 

Edwards Accelerator laboratory, Department of Physics and Astronomy, Ohio University, Athens, Ohio 45701, USA

R. C. Haight

P-3, Los Alamos National Laboratory, Los Alamos, New Mexico 87545, USA



(Received 16 February 2021; revised 13 December 2021; accepted 7 April 2022; published 24 May 2022; corrected 26 May 2023)

The $^{10}\text{B}+n$ system has been studied by measuring charged particles from neutron-induced reactions in the 1 to 20 MeV energy range. Protons, deuterons, tritons, and α particles were measured at four angles using the pulsed white neutron spectrum at the Los Alamos Neutron Science Center Weapons Neutron Research facility. Differential cross sections for each species are reported. These new data are combined with literature data in an R -matrix analysis of the ^{11}B compound system. A comparison is made to the molecular and cluster states candidates observed in these reactions.

DOI: [10.1103/PhysRevC.105.054612](https://doi.org/10.1103/PhysRevC.105.054612)

I. INTRODUCTION

The $^{10}\text{B}(n, Z)$ reactions are important for nuclear science and nuclear engineering, where (n, Z) refers to neutron reactions that result in light charged particles. The $^{10}\text{B}(n, \alpha)$ reaction, for example, is established as a neutron cross section standard from thermal energies to 1.0 MeV [1]. Neutron monitoring is often done using this reaction with BF_3 proportional detectors. As the $^{10}\text{B}(n, \alpha)$ reaction has a large positive Q value and is easily detected, there is interest in extending the neutron standard to higher energies [2]. The $^{10}\text{B}(n, \alpha)$ reaction has been studied and analyzed by a number of authors [3–8].

The proton channel has been less studied. The proton channel, $^{10}\text{B}(n, p_0)^{10}\text{Be}$, is open at thermal energies and could compete with the α channel. A measurement at thermal energies was done by Lal *et al.* [9,10]. There are earlier results at 14 MeV [11]. The measurement of the integrated cross section for the inverse reaction, $^{10}\text{Be}(p, n)^{10}\text{B}$ is available [12]. There are also unpublished results of the same reaction at higher energies at the Ohio University Accelerator Laboratory.

The deuteron channel has been observed at 14 MeV [13] and has also been studied from the inverse reaction $^9\text{Be}(d, n_0)^{10}\text{B}$ in several works [14–21].

Triton production was studied in the early days of nuclear physics and is interesting as a three-body final state reaction. Initial studies were carried out by Chadwick and Goldhaber [22] and Taylor [23]. These initial studies with a Po(Be) source showed “star” features from the $^{10}\text{B}(n, t)\alpha + \alpha$ reaction in photographic plates in addition to the single tracks from the $^{10}\text{B}(n, \alpha)$ reaction. Davis [4] and Valcovič [13,24] measured the $^{10}\text{B}(n, t)$ channel but these measurements were unable to determine the actual reaction

pathway, three body break up, or the two-body sequential reactions $^{10}\text{B}(n, t)^8\text{Be}(0.0) \Rightarrow \alpha + \alpha$ or $^{10}\text{B}(n, t)^8\text{Be}(3.1) \Rightarrow \alpha + \alpha$. The inclusive cross section at thermal for $^{10}\text{B}(n, t)$ reaction has been measured by Kavanagh and Marcle [25] and Clarke and Fleming [26].

Neutron-induced reactions on ^{10}B have been studied via inverse reactions such as $^7\text{Li}(\alpha, n)^{10}\text{B}(g.s.)$. Other inverse reactions that relate to $^{10}\text{B}(n, Z)$ are $^9\text{Be}(d, n_0)$ (as above) and $^{10}\text{Be}(p, n_0)$.

Reactions of this type are often analyzed with an R -matrix analysis that treats the reaction as going through states in the compound nucleus ^{11}B . Our work is timely in that the nuclear levels of $A = 8, 9, 10$, and 11 nuclei have been recently been evaluated [27–29]. The present (n, Z) results together with other measurements including elastic and inelastic neutron scattering are the inputs to the R -matrix analysis presented here.

R -matrix fitting is a very useful tool for performing evaluations and extracting level parameters such as resonance energies, partial widths, spins and parities. It is helpful to have data for as many channels as possible, with the channels with large cross section being most important. The total neutron cross section, angle-integrated cross sections, and differential cross sections are all useful for constraining the fit. Differential cross section data are more useful than angle-integrated data, as they are more sensitive to the spin and parity of the states in the compound nucleus.

II. EXPERIMENTAL

The $^{10}\text{B}(n, Z)$ reactions were investigated using the spallation neutron source at the Weapons Nuclear Research Facility (WNR) at the Los Alamos Neutron Science Center (LAN-SCE) [30]. The experiment was performed in the so-called NZ chamber, shown in Fig. 1, located at the 15.1-m station on the 30°-right beam line. The neutron flux at low energies

*massey@ohio.edu

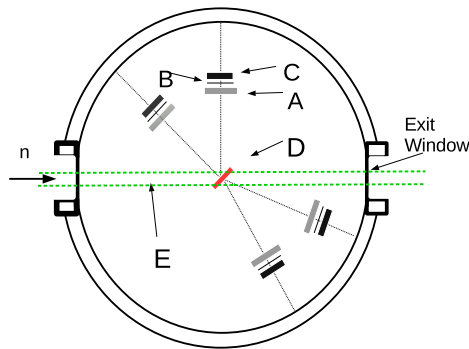


FIG. 1. The NZ chamber experimental setup at the 15.1 meter station. The ΔE - E detectors are shown with the proportional counter (A), the collimator (B), and the 450 mm²-area 250- μ m-thick silicon detector (C). The target (D) is shown with the target material facing the 20° and 60° detectors. The neutron beam (E) travels through the chamber from left to right. For data taking with the 90° and 135° detectors, the target was rotated by 180°, such that the target material faced the more backward angle detectors. The detectors were shielded in the chamber with ≈ 10 cm of copper in the upstream direction to reduce the neutron-induced background.

was reduced during most of the experiment by a polyethylene filter that was placed upstream in the neutron beam.

The neutron yield was monitored by a ²³⁵U fission chamber located downstream from the (n, Z) chamber at a distance of 16.27 m from the neutron source.

The neutron source was pulsed with a pulse spacing of 1.8 μ s for which the overlap neutron energy was 0.37 MeV at the (n, Z) chamber. The minimum neutron energy used in this work is 800 keV. Overlap neutrons did not impact the charged-particle measurements as the reactions with low-energy neutrons produce energy signals below the energy of interest for this work. For the fission chamber, the contribution of the overlap neutrons is expected to be very small in the energy region of interest based on previous experience and the observed fission time-of-flight spectrum. The diameter of the neutron beam exiting the chamber was measured as 22.3 ± 1.0 mm using radiography.

The fission chamber used was the “B” chamber described in Refs. [31,32]. The ²³⁵U deposit is 13.3 cm in diameter and consists of 65 mg of uranium. The isotopic composition of the fission deposit was ²³⁴U, 0.26%; ²³⁵U, 98.20%; ²³⁶U, 0.937%; and ²³⁸U, 0.595%. The neutron yield measured by the fission chamber is shown in Fig. 2.

The ¹⁰B target was produced by electron-beam evaporation of isotopically enriched boron on to a 0.05-mm-thick tantalum substrate. The thickness of the boron layer was chosen to be optimal for measuring outgoing protons from the ¹⁰B(n, p) reaction, and was measured to be 2.5 ± 0.38 μ m using a quartz crystal thickness monitor during the deposition. The boron deposit was 50 mm in diameter and centered on the tantalum substrate. The boron was enriched to 99.82 atomic percent of ¹⁰B and was obtained from Eagle-Pitcher lot #MF9110-AY [33].

The NZ chamber was developed to study neutron induced-reactions over the wide energy range available at the WNR

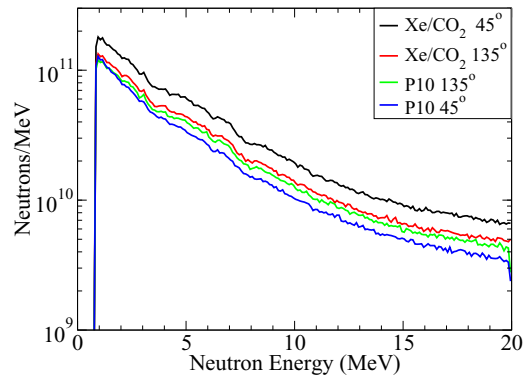


FIG. 2. Neutron yields at the fission chamber for each target orientation and gas filling of the chamber. They are in order from top to bottom, Xe/CO₂ at 45° (black), Xe/CO₂ at 135° (red), P10 gas at 135° (green), and P10 gas at 45° (blue). The 45° orientation with P10 gas filling had some of the data taken with the polyethylene filter out.

spallation source [34,35]. For this experiment a thin-window proportional counter and a silicon detector were used at each angle as a ΔE - E telescope for particle identification. The entire chamber was filled with counting gas to reduce the stress on the proportional detector windows. This also removed the need for the proportional detectors to be leak tight. The entrance window for this chamber was a 0.3-mm-thick molybdenum foil while the exit foil was a 0.2-mm-thick Mylar window.

The silicon detectors were 250- μ m thick, which is sufficient to stop 5.5-MeV protons, 8.0-MeV tritons, and 22.5-MeV α particles. A 2.24-cm-diameter collimator was placed in front of each silicon detector to define the solid angle and eliminate edge effects in the silicon detector. The entrance and exit windows of the proportional counter were 0.013-mm-thick aluminized Mylar. The detector setup measurements are given in Table I. The outgoing charged particles were detected at 20°, 60°, 90°, and 135°. These detectors were shielded with copper blocks of at least 10-cm thickness to reduce the background from scattered neutrons.

Two separate gas fillings of the chamber were used for the proportional detectors. Roughly half of the data was taken with each gas filling. Initially a filling of 34 torr of P10 gas (90% Ar, 10% CH₄) was used. The background rate from the H(n, n)H reaction was much larger than the contribution of

TABLE I. Physical parameters for the detector setup. The distance was measured from the target to the collimator.

Nominal Detector Angle (degrees)	Distance Target to Collimator (cm)	Solid Angle (sr)	Opening Angle (degrees)
20	17.4	0.0130	7.366
60	15.6	0.0162	8.213
90	14.9	0.0178	8.597
135	14.1	0.0198	9.083

TABLE II. Thresholds and spin parities of the final level for reactions in the $n + {}^{10}\text{B}$ system. The energies are from the most recent evaluations [27–29].

Reactions	J^π	Q Value (MeV)	Threshold (MeV)
${}^{10}\text{B}(n, n_0){}^{10}\text{B}(0.000)$	3^+	0.000	0.000
${}^{10}\text{B}(n, n_1){}^{10}\text{B}(0.718)$	1^+	-0.718	0.791
${}^{10}\text{B}(n, n_2){}^{10}\text{B}(1.740)$	0^+	-1.915	1.915
${}^{10}\text{B}(n, n_3){}^{10}\text{B}(2.154)$	1^+	-2.371	2.371
${}^{10}\text{B}(n, n_4){}^{10}\text{B}(3.587)$	2^+	-3.948	3.948
${}^{10}\text{B}(n, p_0){}^{10}\text{Be}(0.000)$	0^+	0.2258	0.000
${}^{10}\text{B}(n, p_1){}^{10}\text{Be}(3.368)$	2^+	-3.142	3.368
${}^{10}\text{B}(n, p_2){}^{10}\text{Be}(5.958)$	2^+	-5.733	6.309
${}^{10}\text{B}(n, p_3){}^{10}\text{Be}(5.960)$	1^-	-5.734	6.311
${}^{10}\text{B}(n, d_0){}^9\text{Be}(0.000)$	$3/2^-$	-4.3612	4.801
${}^{10}\text{B}(n, d_1){}^9\text{Be}(1.684)$	$1/2^-$	-6.046	6.654
${}^{10}\text{B}(n, d_2){}^9\text{Be}(2.429)$	$5/2^-$	-6.791	7.475
${}^{10}\text{B}(n, t_0){}^8\text{Be}(0.000)$	0^+	0.2307	0.000
${}^{10}\text{B}(n, t_1){}^8\text{Be}(3.030)$	2^+	-2.850	3.081
${}^{10}\text{B}(n, \alpha_0){}^7\text{Li}(0.000)$	$3/2^-$	2.7902	0.000
${}^{10}\text{B}(n, \alpha_1){}^7\text{Li}(0.478)$	$1/2^-$	2.312	0.000
${}^{10}\text{B}(n, \alpha_2){}^7\text{Li}(4.630)$	$7/2^-$	-1.862	2.049
${}^{10}\text{B}(n, \alpha_3){}^7\text{Li}(6.680)$	$5/2^-$	-3.814	4.197
${}^{10}\text{B}(n, \alpha_4){}^7\text{Li}(7.454)$	$5/2^-$	-4.664	7.324
${}^{10}\text{B}(n, \alpha_5){}^7\text{Li}(8.75)$	$3/2^-$	-5.960	9.360
${}^{10}\text{B}(n, \alpha_6){}^7\text{Li}(9.09)$	$1/2^-$	-6.30	9.90
${}^{10}\text{B}(n, \alpha_6){}^7\text{Li}(9.57)$	$7/2^-$	-7.78	10.655

either the ${}^{10}\text{B}(n, p)$ or ${}^{10}\text{B}(n, t)$ reactions. A filling with a mixture of 20 torr of a 90.1% Xe and 9.9% CO_2 was used

to reduce the background for the proton (p), deuteron (d), and triton (t) outgoing particles.

The background from charged-particle production in the gas was considered based on the elemental abundance and Q value. The major background is expected from carbon and oxygen in the gas. The major isotope of carbon and oxygen have large negative Q values for (n, α) . The minor isotopes also have negative Q values except for ${}^{17}\text{O}$ which has a Q value for ${}^{17}\text{O}(n, \alpha){}^{14}\text{C}(0.0)$ of 1.81 MeV with an abundance of 0.04%. The reactions ${}^{10}\text{B}(n, \alpha_0){}^7\text{Li}(0.0)$ and ${}^{10}\text{B}(n, \alpha_1){}^7\text{Li}(0.478)$ have large positive Q values as shown in Table II and none of the neutron induced reactions in the gas can produce background α particles. The Q values for the emission of proton, deuteron, and triton are all negative and high for the carbon and oxygen isotopes. The background from the gas should thus be at energies below the reactions studied for the p, d, and t particles. The background from argon and xenon was expected to be small due to their low cross sections. Any contributions from the gas are subtracted using the sample-out runs. There may be some water in the sample due to absorption from air. This should have only a small effect due to the low cross section for α production for natural oxygen.

The outgoing charged particles were detected at laboratory angles of 20° , 60° , 90° , and 135° . The ΔE versus E plots for the P10 and Xe fillings of the proportional detectors are shown in Figs. 3 and 4. The details of the detector telescopes are shown in Fig. 1 and Table I.

The thick tantalum backing allowed the boron deposit to be seen by only one set of detectors at a time. Two target orientations were used in this experiment, with the target rotated to either 45° or 135° relative to the neutron beam direction.

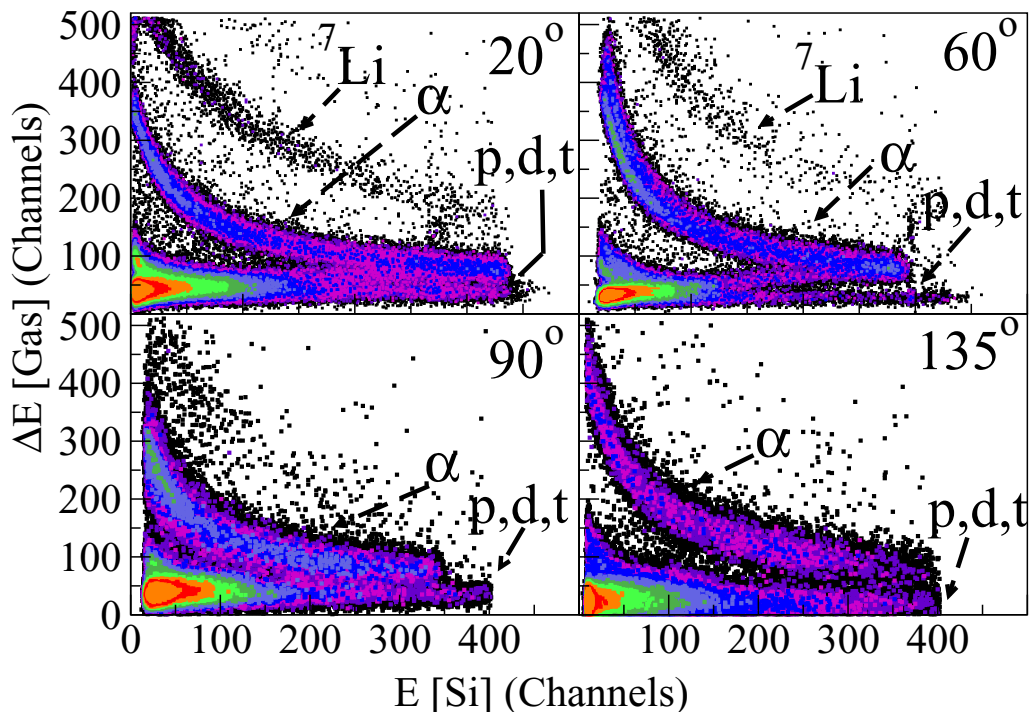


FIG. 3. ΔE versus E for the P10 gas for neutron energies below 20 MeV.

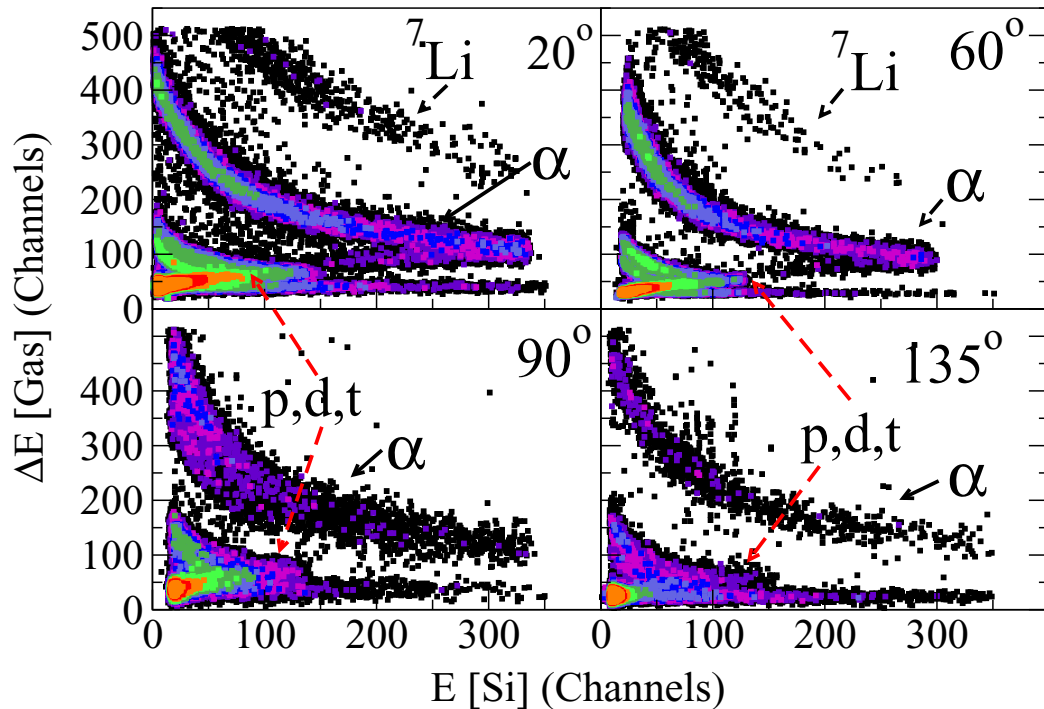


FIG. 4. ΔE versus E for the Xe/CO₂ gas for neutron energies below 20 MeV.

These orientations allowed either the forward or the backward detectors to see the boron target. A background measurement was made when the back of the target faced the detectors. Nearly equal times were used for measuring foreground and background spectra.

The signals from the proportional counters, the silicon detectors, and the fission chamber were digitized by a fast encoding and readout analogue-to-digital converters (FERA) developed by LeCroy Research Systems Corporation. The time-of-flight signals were determined by using start signals from the detectors and stop signals from a delayed timing signal from the accelerator. A LeCroy module with a MTD133B chip was used to digitize the time-of-flight, with 0.5 ns/channel. An oscillator used in this chip precisely determines the time interval between every eight channels. The time intervals for the seven intermediate channels are then interpolated.

The data were acquired in event mode using the XSYS [36] data acquisition system using a VAX computer. The data were collected in event mode, ΔE , E , and time-of-flight (E -TOF) relative to the accelerator beam pick-off signal. Two-dimensional plots of ΔE versus E were available on line to check the particle identification. In replaying the event-mode data, events were sorted according to gates placed around the particle of interest in the two-dimensional pulse height arrays, ΔE versus E_{Si} and E_{Si} versus time-of-flight. To replay the low-energy proton and deuteron data, it was necessary to eliminate charged-particle events where the particles did not stop in the Si detector and hence did not deposit their full energy. A particle maximum energy was calculated from the gas filling and the silicon thickness. The energy of this particle is used to limit the maximum neutron energy reported for each channel.

III. ANALYSIS

A preliminary analysis of some of the experimental data was presented in Refs. [37,38]. Several improvements in the analysis have subsequently been implemented and the present work is the final analysis of the full data set.

The data were analyzed using the HRIBF UPAK software package [39]. The SCANOR subroutines from this software package were modified to replay and analyze the data using two-dimensional gates set on the ΔE - E and E -TOF plots.

The initial step in the analysis was to correct for intermittent shifts in the neutron timing signal. Some of these shifts were observed to be from tuning of the accelerator. A further component was likely the temperature change in the data acquisition area. The correction was performed by replaying the data in segments large enough to determine the centroid of the γ -ray peak to within 1 channel. Each segment was then shifted to a set channel to align it in time with the previous segments. This procedure yielded data sets for each experimental configuration that were much simpler to analyze.

A. Time correction

The measured time is from the detection of a charged particle in the silicon detector and the delayed accelerator timing signal. The neutron time of flight from the source to the sample is calculated from the time between the accelerator timing pulse and the detection of the charged particle, with a correction for the time of flight from the sample to the charged-particle detector. The first step is to identify the outgoing particle. The α s are well separated from protons, deuterons, and tritons in the particle identification plots Figs. 3

TABLE III. Gamma-ray widths of the silicon and fission detectors.

Detector	P10 FWHM (ns)	Xe/CO ₂ FWHM (ns)
20°	4.0(5)	4.0(5)
60°	3.0(5)	4.0(5)
90°	5.5(5)	5.5(5)
135°	5.0(5)	5.0(5)
Fission chamber	5.0(5)	5.0(5)

and 4. The proton, deuteron, and triton particles could only be separated using both ΔE - E and E -TOF gates.

Time corrections were calculated using the known composition of the gas, the distance to the detectors, and the thickness of the target. The silicon detector energy was calibrated using a $^{228}\text{Th}/^{229}\text{Th}$ α source. The energy loss of the particle in the target, the gas, and the aluminized Mylar was calculated using the energy loss tables from Ziegler [40].

The time of flight and particle energy were calculated from the kinematics of each reaction. The particles were taken as originating at the back of the target, the middle of the target, or the front face of the target. Both the time of flight of the emitted particle and energy deposited in the silicon detector were calculated from the energy losses. The energy deposited in the silicon detector was then used to interpolate the time of flight of the particle for each event assuming it originated in the middle of the target. The difference of the time of flight through the entire target and from the face of it were used to estimate the error in the time of flight calculation. The overall error in this procedure was estimated to be ~ 2 ns from this analysis including the error in the silicon detector calibration.

The neutron time of flight is then calculated relative to the γ peak in each detector. The width of the γ peaks for each detector used in the experiment is shown in Table III.

B. Gates on E -TOF

The determination of the gates for each reaction channel was made using the information about the experimental set up, the detector calibrations, and the reactions kinematics. The kinematic calculations for each reaction gave the neutron energy, and the outgoing particle energy for each angle. The energy loss was calculated using the central angle of each detector. The angular acceptance range for the detector was neglected in this modeling. The energy loss for an outgoing particle through the target, the gas and the aluminized Mylar was calculated using the energy loss tables from Zeigler [40]. The energy deposited in the silicon was also calculated. The energy deposited in the silicon detector for a particle with a given initial energy passing through full target thickness was taken as the minimum energy for a gate. The energy deposited in the silicon detector of a given initial particle energy for particle originating at the surface of the target was taken the maximum energy for a gate. These results were converted to channels using the neutron energy, and the silicon detector, and time of flight calibrations. This procedure gave gates for each reaction channel.

Plots of E -TOF are shown in Figs. 5–7, respectively. We are able to distinguish between the $^{10}\text{B}(n, p_0)$ and $^{10}\text{B}(n, t_0)$ using gates on the E versus TOF plots.

A further consistency check on the gates was done by the comparison of the results from each of the gas fillings. The cross sections for each reaction were calculated each for angle and each gas filling. The comparison of these results were within error bars for all but the 20 degree $^{10}\text{B}(n, t_0)$ reactions. The results from each gas filling were averaged to give the final results. The comparison of the data from each of the gas fillings for the $^{10}\text{B}(n, \alpha_{0+1})$ reaction is discussed below.

The energy loss of the α particles exiting the target is significant. For 1-MeV incident neutrons, the α_0 energy exiting normal to the plane of the target can be reduced from 2.906 to 2.18 MeV depending on where the α particle is produced in the sample. For the α_1 peak the energy is reduced from 2.567 to 1.78 MeV. Using a target of this thickness does not allow resolution of the $^{10}\text{B}(n, \alpha_0)$ $^7\text{Li}(g.s)$ and $^{10}\text{B}(n, \alpha_1)$ $^7\text{Li}(0.478)$. While these reactions cannot be separated, the sum of the channels is well determined, as shown in Fig. 5.

The $\text{H}(n, n)\text{H}$ scattering was greatly reduced in the switch from the P10 gas to the Xe/CO₂ gas fill but was still visible in the plots. The energy loss in the gas was important to the quality of the data. The triton group has very close to the same positive Q value as the protons as shown in Table II. The separation of the triton group from the $\text{H}(n, n)\text{H}$ scattering was better in the Xe/CO₂ E -TOF plot as amount of hydrogen in the gas was much reduced. The ΔE - E spectrum does not have full separation of proton and tritons. A partial separation of protons from tritons was obtained at 20° with the Xe/CO₂ filling by making ΔE - E plots by gating on clear proton and triton groups in the E -TOF spectrum. The protons and tritons groups could each be gated but with an overlap region in this ΔE - E spectrum. The result of this procedure is shown in Fig. 8. This greatly reduced the background from $\text{H}(n, n)\text{H}$ scattering at 20°. The final separation of the tritons from background at 20° was done by careful gating on the E -TOF spectrum. At the other angles the data from both fillings were comparable and were added in the final data.

We were able to identify the additional charged-particle groups $^{10}\text{B}(n, \alpha_2)$, $^{10}\text{B}(n, \alpha_3)$, $^{10}\text{B}(n, p_1)$, and $^{10}\text{B}(n, t_1)$. The gates were calculated as above and slightly widened to account for the angular acceptance and target thickness. These channels have a modest background. The beam-induced background measured with the rotated-target runs was subtracted.

The data were sorted in neutron energy bins with widths of 0.1 to 0.5 MeV. The widths were chosen to provide good statistical accuracy while not masking any short-range structure which might be present in the cross section.

C. Cross section calculation

The fission chamber deposit had $N_U = (1.20 \pm 0.02) \times 10^{18}$ U atoms/cm². The isotopic composition of the uranium deposit was 0.595% ^{238}U , 0.937% ^{236}U , 98.208% ^{235}U , and 0.26% ^{234}U [31,32]. The boron target was determined to have $N_B = (3.3 \pm 0.5) \times 10^{20}$ ^{10}B atoms/cm². The differen-

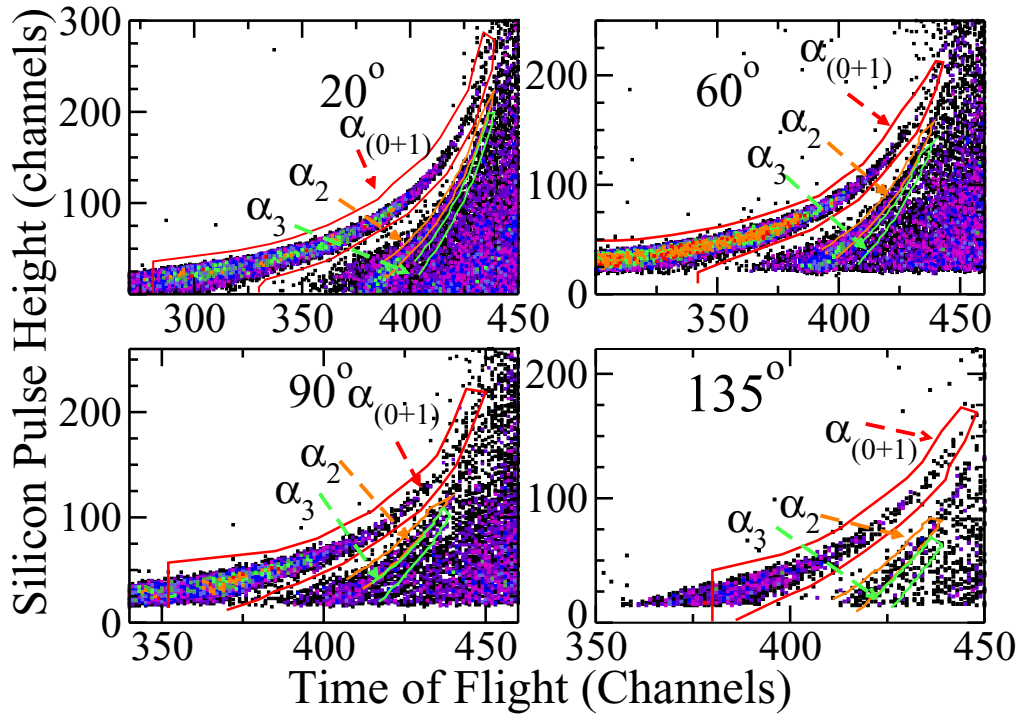


FIG. 5. The silicon detector pulse height versus TOF for the P10 filling is shown compressed of 8 in time of flight and a factor of 2 in pulse height for all detectors with a gate on the α groups in the ΔE versus E_{Si} plot. The gates used for $^{10}\text{B}(n, \alpha_{0+1})$ are shown in red. The calculated gates for $^{10}\text{B}(n, \alpha_2)^7\text{Li}(4.630)$ (orange) and $^{10}\text{B}(n, \alpha_3)^7\text{Li}(6.680)$ (green) are shown. The TOF increases to the left with 4 ns per channel. The lowest value in this plot is a single count.

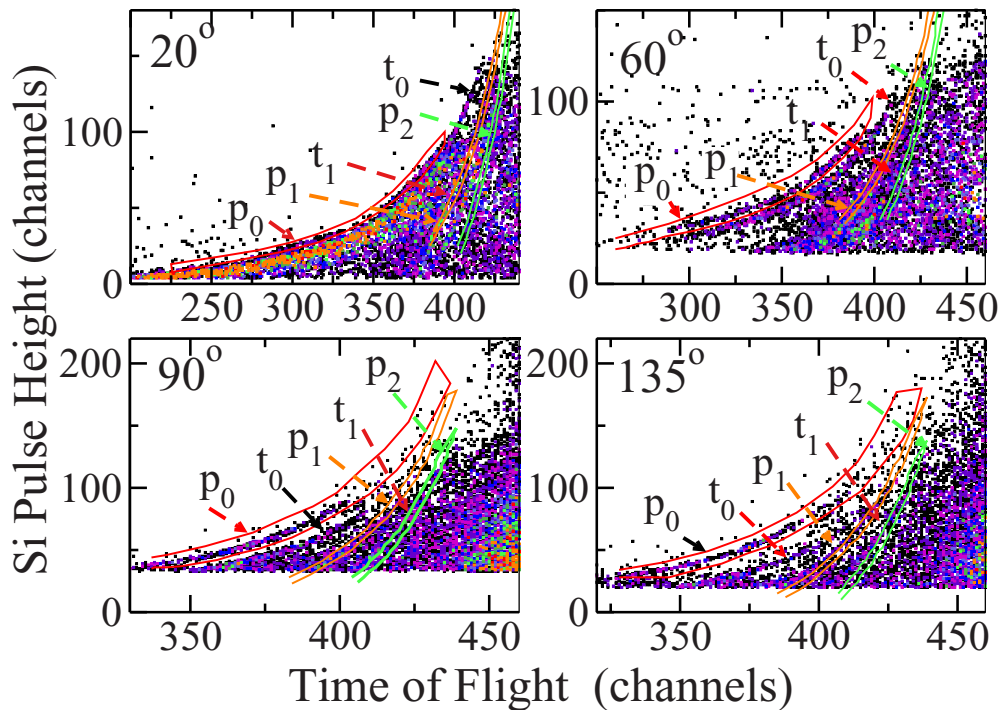


FIG. 6. The Silicon detector pulse height versus TOF for the P10 filling is shown compressed by a factor of 8 in energy and a factor of 2 in pulse height for all detectors with a gate on hydrogen group in the ΔE versus E_{Si} plot. The gates used for $^{10}\text{B}(n, p_0)^{10}\text{Be}(g.s.)$ (red) reaction, and the calculated gates for $^{10}\text{B}(n, p_1)^{10}\text{Be}(3.368)$ (orange), and $^{10}\text{B}(n, p_2)^{10}\text{Be}(5.9)$ (green) reactions are shown. The contribution $^{10}\text{B}(n, t_0)^8\text{Be}(g.s.)$ and $^{10}\text{B}(n, t_1)^8\text{Be}(3.030)$ reactions are indicated. The TOF increases to the left with 4 ns per channel.

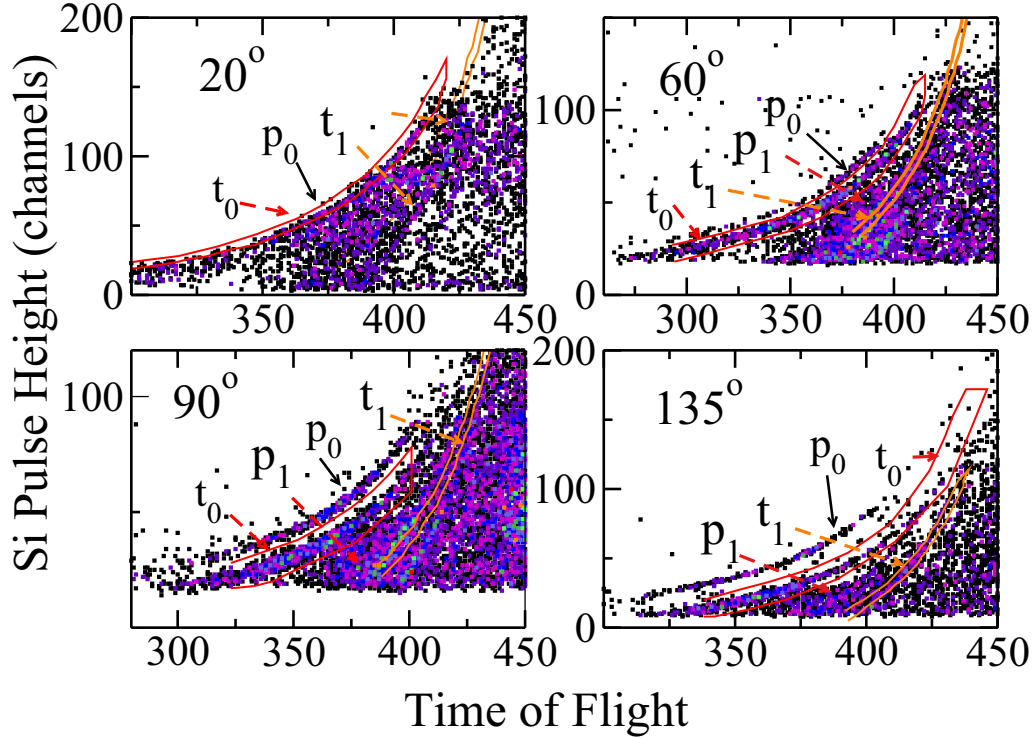


FIG. 7. The Silicon detector pulse height versus TOF for the P10 filling is shown compressed by a factor of 8 in time of flight and a factor of 2 in pulse height for all detectors with a gate on triton group in the ΔE versus E_{Si} plot. The gates used for $^{10}\text{B}(n, t_0)^8\text{Be}(g.s.)$ (red), $^{10}\text{B}(n, t_1)^8\text{Be}(3.030)$ (orange). The contributions from the $^{10}\text{B}(n, p_0)^{10}\text{Be}(g.s.)$ and the $^{10}\text{B}(n, p_1)^{10}\text{Be}$ reactions are indicated. There is only a small contribution from the $^{10}\text{B}(n, p_0)$ reaction at 20 degrees due to the refined gating on the ΔE - E spectrum. The TOF increases to the left with 4 ns per channel.

tial cross section was determined using

$$\frac{d\sigma(E_n)}{d\Omega} = \frac{C_B(E_n)\epsilon_f N_U \sigma_U(E_n)}{C_f(E_n)\epsilon_B N_B \Delta\Omega}, \quad (1)$$

where C_f is the number of fission counts, C_B is the number of counts in the Si telescope, ϵ_f is the efficiency of the fission chamber, ϵ_B is the efficiency of the Si telescope, and $\sigma_U(E_n)$ is the fission cross section. The solid angle, $\Delta\Omega$ is taken

from Table I. We take $\epsilon_f = 0.98$ to take into account the number of events lost below the threshold used for the fission chamber [31,32]. We assume $\epsilon_B = 0.98$.

We used cross sections for (n, f) for the uranium isotopes from the ENDF/B-VII.1 evaluation [41], averaged over the neutron energy distribution in the energy bin. The differences between the ENDF/B-VII.1 evaluation used and the current ENDF/B-VIII.0 [42] evaluation are less than 1% over the 1–20 MeV range of the experimental measurements.

The cross section calculation can also be written as

$$\frac{d\sigma(E_n)}{d\Omega} = \frac{C_B(E_n)}{C_f(E_n)\Delta\Omega} \times \text{constant}, \quad (2)$$

where the factors that are constant across the data set are combined into a single constant. The systematic uncertainties in the composition of the target, the uranium deposits of the fission chamber, the efficiency of the fission chamber, and the detector efficiency can then be reduced to a single normalization error. These known sources of uncertainties are shown in Table IV. The systematic uncertainties from the fission detector and the target thickness may be reduced if a normalization to a higher precision work is made in the future.

There are other uncertainties in the experiment that are more difficult to quantify. These include: the choice of the charged-particle gates used for each reaction channel, the correction of the neutron time-of-flight, the correction of time shifts in the fission spectra, and the ^{235}U isotopic composition.

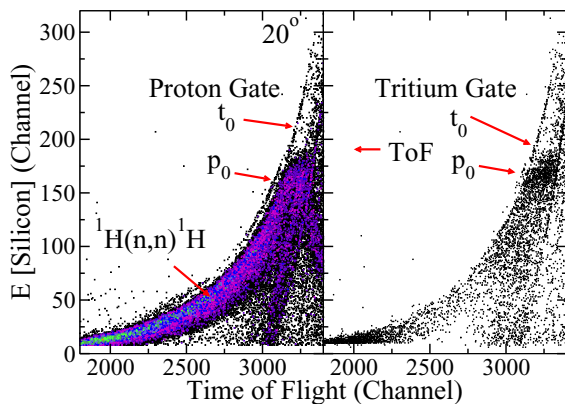


FIG. 8. Plots of the time-of-flight (horizontal axis) versus silicon pulse height (vertical axis) for 20° and Xe/CO₂ gas for both the proton and triton ΔE - E gates. The pulse height has been compressed by a factor of 2 and the time of flight is 0.5 ns/channel.

TABLE IV. Values and estimates of systematic uncertainties.

Source	Value	Percent uncertainty
Fission chamber		
Efficiency	0.98	2.0
Fission deposit		
Thickness [31,32]	0.468 $\frac{\text{mg}}{\text{cm}^2}$	1.5
	$1.20 \times 10^{18} \frac{\text{atoms}}{\text{cm}^2}$	
Silicon detector		
Efficiency	0.98	2.0
Solid angle		
20°	13.0 msr	1.0
60°	16.2 msr	1.0
90°	17.8 msr	1.0
135°	19.8 msr	1.0
^{10}B target		
thickness	2.5 μm	15.0
	$3.3 \times 10^{20} \frac{\text{atoms}}{\text{cm}^2}$	15.0

Possible sources of background in the experiment are from the target backing, impurities in the target, and the gas used in gas filling. For particles in the hydrogen band this can also come from incomplete separation in the ΔE - E gate. The background from the target backing has been determined by measuring the blank side of the target while the side with the ^{10}B is being measured by the opposite detectors. This allows subtraction of background from the backing, the gas and events in the silicon detectors. The possible contribution of the gases used is discussed above. There may be water absorbed in the target. This should contribute to the $\text{H}(n, n)\text{H}$ background. The contributions from oxygen are expected to be very small. There are no other clear kinematic bands other than beyond those expected from neutron induced reactions on ^{10}B and $\text{H}(n, n)\text{H}$ scattering.

The background from neutron scattering from $\text{H}(n, n)\text{H}$ is strong for the 20° detector. This background impacted the measurement for p, d, and t particles. The $^{10}\text{B}(n, p_0)^{10}\text{Be}$ reaction was least affected due to the positive Q -Value. The $^{10}\text{B}(n, t_0)^8\text{Be}$ reaction also has a positive Q value but its energy loss reduces the triton energy enough to be close to $\text{H}(n, n)\text{H}$ scattering. The 20° tritons are partially separated in the ΔE - E plots from the protons only for the Xe/CO₂ filling. There is a possible background from the $\text{H}(n, n)\text{H}$ scattering of concern at the energies of 3–5 MeV in the $^{10}\text{B}(n, t_0)$ measurement at 20°. The $^{10}\text{B}(n, d_0)^9\text{Be}$ gate is in the continuum from the $\text{H}(n, n)\text{H}$ scattering at 20°

The $^{10}\text{B}(n, p_1)$ and $^{10}\text{B}(n, t_1)$ reactions have very similar Q values. They are only separated in this experiment by their difference in energy loss in the gas. Their calculated gates overlap for the forward angles of 20° and 60°. In addition, the $\text{H}(n, n)\text{H}$ scattering at 20° also prevents any differential cross section for these reactions to be determined. These two reactions are only separated in the 90° and 135° detectors.

The kinematic band for the $^{10}\text{B}(n, d_0)$ has a continuum of background from $\text{H}(n, n)\text{H}$ scattering at 20°. In spite of this, the comparison of the results for a Xe/CO₂ and P10 gas

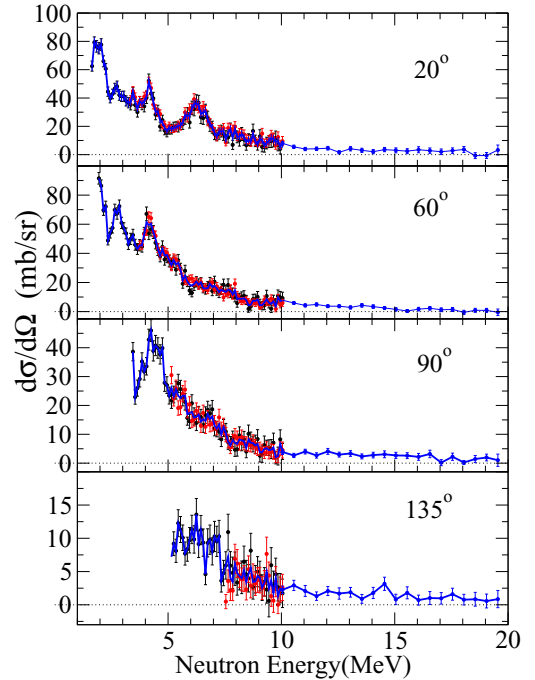


FIG. 9. A comparison of the experimental measurements of ^{10}B , (n, α_{0+1}) cross sections for each gas filling below 10 MeV. The points in black are from the P10 filling, the red points are from the Xe/CO₂ filling and the blue line is the average to the two data sets with binning of 100 keV below 10 MeV. There is little structure above 10 MeV and the results have been combined. The bins are chosen to be 500 keV bins and only the average values are shown in blue.

are within error bars at this angle. The $\text{H}(n, n)\text{H}$ background changes dramatically between the two fillings as discussed above. The continuum background from $\text{H}(n, n)\text{H}$ scattering is a factor of five lower in the Xe/CO₂ than the deuterium band at 20° with the P10 gas mixture. The cross sections at 20° were consistent within error bars for both fillings despite a large change in the background.

IV. CROSS SECTION RESULTS

The four point angular distributions of the $^{10}\text{B}(n, \alpha_{0+1})$, $^{10}\text{B}(n, \alpha_2)$, $^{10}\text{B}(n, \alpha_3)$, $^{10}\text{B}(n, p_0)$, and $^{10}\text{B}(n, t_0)$ reactions have been measured. Limited results were obtained for $^{10}\text{B}(n, p_1)$, $^{10}\text{B}(n, t_1)$, and $^{10}\text{B}(n, d_0)$

The $^{10}\text{B}(n, \alpha_{0+1})$ group has only a few counts of background over the full range of angle and energies as shown in Fig. 5. The $^{10}\text{B}(n, t_0)$ data have background in the 20° detector from the $^1\text{H}(n, n)$ reaction. This background continues up to and may overlap the data taken with the Xe/CO₂ gas filling. The shape of this background makes it difficult to estimate near 5 MeV where the protons no longer stop in the silicon detector. All of the data taken with P10 gas were compared those taken with the Xe/CO₂ mixture. This comparison showed consistent results for all of the detectors.

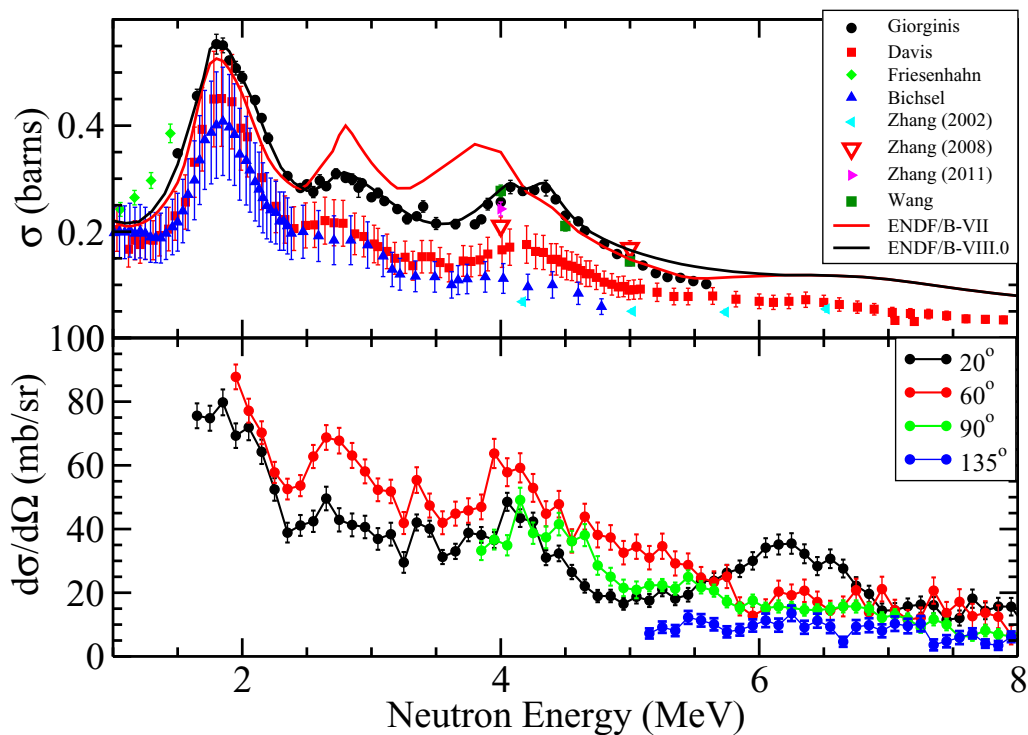


FIG. 10. A comparison of the experimental measurements of $^{10}\text{B}(n, \alpha_{0+1})$ cross sections. The angle integrated cross section data shown in the uppermost plot are taken from Giorginis and Khryachkov [7] (solid black circles), Davis *et al.* [4] (solid red squares), Bichsel and Bonner [3] (dark blue triangles), Friesenhahn *et al.* [43] (green diamonds), Zhang *et al.* [44] (left facing cyan triangles), Zhang *et al.* [45] (open red downward pointing triangles), Zhang *et al.* [46] (magenta triangles), and Wang *et al.* [47] (green squares). The lower figure shows the current differential cross sections, 20° (black), 60° (red), 90° (green), and 135° (blue).

A. The $^{10}\text{B}(n, \alpha_0)$ and $^{10}\text{B}(n, \alpha_1)$ reactions

In this experiment, the $^{10}\text{B}(n, \alpha_0)$ and $^{10}\text{B}(n, \alpha_1)$ cross sections could not be separated completely due to the large energy loss in the ^{10}B target. A comparison of the results with the P10 filling and the Xe/CO₂ filling is shown in Fig. 9. This shows the good agreement in the cross section and energy for these two sets of data. The current results, the previous reported data, and the current evaluation are shown in an expanded scale in Fig. 10.

The energy dependence of the measured differential cross section of $^{10}\text{B}(n, \alpha_{0+1})$ in this experiment may give some insight into the problems in evaluating the α channels in the $^{10}\text{B}+n$ compound system. The comparison of the previous data with the current evaluation is shown in Fig. 10.

There has been an outstanding problem of discrepancies between different experiments on α s produced by neutrons interacting with ^{10}B for energies above 2 MeV. This is shown in Fig. 10. The current results indicate that the angular distribution may help understand the results of the differing experiments. The cross section at 135° is the lowest for all energies where it is above threshold. This indicates that the differential cross sections at forward angles are likely to be larger than the backward cross sections in the entire energy range.

Several previous experiments investigating the $^{10}\text{B}(n, \alpha)^7\text{Li}$ channel in this energy region have used gas targets for the measurement [3,4,6–8,46]. These methods

can have both good energy resolution and thin targets which allows separation of these two reactions.

The recent results from Wang *et al.* [47,48] and Giorginis and Khryachkov [7] have very good statistics. The experiments of Giorginis *et al.* [7,49] were done with a single Frisch-grid proportional chamber relative to a fission chamber. Their experiment measured only the α particles in the forward hemisphere and was limited to a range 0° to 70° with clean separation of the α and ^7Li groups. The backward angle cross sections were obtained from the ^7Li data. The older work by Davis [4] has poorer statistics but the detection method is simpler and is independent of the angular distribution.

The change in the evaluations from ENDF/B-VIII.0 from ENDF/B-VII for this reaction this reaction is supported the current work. The reduction of the cross section at ≈ 3.5 MeV is consistent with our results where there is a minimum in our data at 20° , 60° , and 90° near this energy.

The differential cross sections determined for sum of the $^{10}\text{B}(n, \alpha_0)$ and $^{10}\text{B}(n, \alpha_1)$ are compared with the published data for the angle-integrated cross sections in Fig. 10. Angular distributions have been measured below the energy range of this experiment [50–52]. The available data in our energy range were from Tang *et al.* [53], Zhang *et al.* [44] who also gave the sum of the same differential cross sections. They measured angular distributions with a gridded proportional chamber. A comparison with these data with the current work is shown in Fig. 11. These data are significantly larger than the previous data and have a different shape of the angular distri-

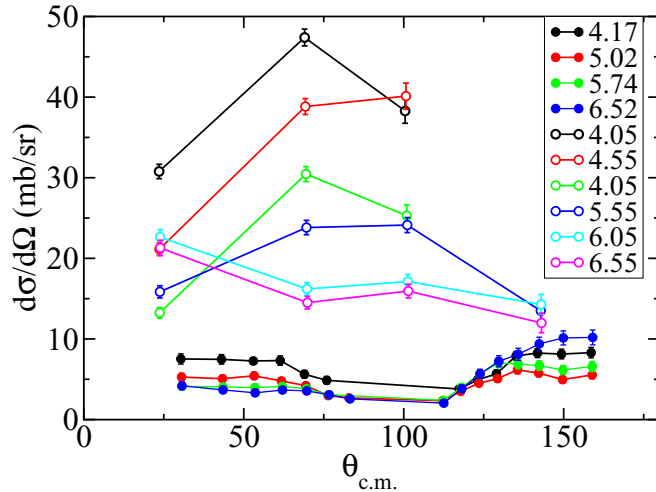


FIG. 11. Angular distributions in the center of mass for $^{10}\text{B}(n, \alpha_0) + ^{10}\text{B}(n, \alpha_1)$ reactions. The data from Zhang *et al.* [44] are shown as solid circles and the current data are shown as open circles.

bution. The shape of the reported angular distribution [44,53] may be influenced in part by particle leakage when using twin Frisch-grid proportional chambers [49]. No angular distributions have been presented by this collaboration in subsequent publications using similar methods [45–48].

The integrated cross sections for sum of the $^{10}\text{B}(n, \alpha_0)$ and $^{10}\text{B}(n, \alpha_1)$ are now in common agreement after corrections for particle leakage [45–48]. A recent measurement using twin Frisch-grid ion chambers has been reported by Hamsch and Ruskov [51]. Their results are for the differential and angle-integrated cross sections at neutron energies less than 1 MeV.

There is a recent publication of cross sections and angular distribution in the range of $1 \text{ eV} \leq E_n \leq 2 \text{ MeV}$ by Jiang *et al.* [54]. This work was done using 15 gas proportional detectors and silicon detectors. Their results with this method are in agreement with previous methods and more accurate than those from a comparable work by Hamsch and Ruskov [51] using a Frisch-grid ion chamber.

B. The $^{10}\text{B}(n, \alpha_2)$ and $^{10}\text{B}(n, \alpha_3)$ reactions

We have measured the differential cross sections for the $^{10}\text{B}(n, \alpha_2)^7\text{Li}(4.630)$ and the $^{10}\text{B}(n, \alpha_3)^7\text{Li}(6.680)$ reaction to neutron energies up to 20 MeV. The contribution of the α s from the decay of the ^7Li state at 4.630 MeV was seen at the lower neutron energies for the $^{10}\text{B}(n, \alpha_2)$ reaction. This resulted in a much steeper slope of the differential cross section at 20° at low energies. These secondary α s could result in some double counting as these α s were in the kinematic cut for the reaction. A cut on the pulse height was used to remove this energy region from the data set. The secondary α s from the $^{10}\text{B}(n, \alpha_3)$ reaction were much less evident. No previously published cross sections were found in the literature for these reactions. These results are shown in Figs. 12 and 13. The cross sections of both the $^{10}\text{B}(n, \alpha_2)$ and the $^{10}\text{B}(n, \alpha_3)$ reactions contribute to both the tritium and helium production cross sections.

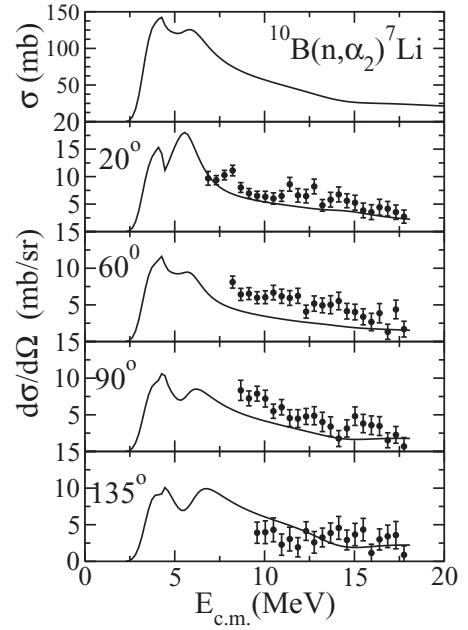


FIG. 12. *R*-matrix fits to the differential cross section for the $^{10}\text{B}(n, \alpha_2)$ reaction in the center of mass system. The results in the center of mass are labeled with the detector laboratory angle. The integrated cross section determined from the fit is shown in the uppermost panel. The lower figure shows our results for the differential cross sections.

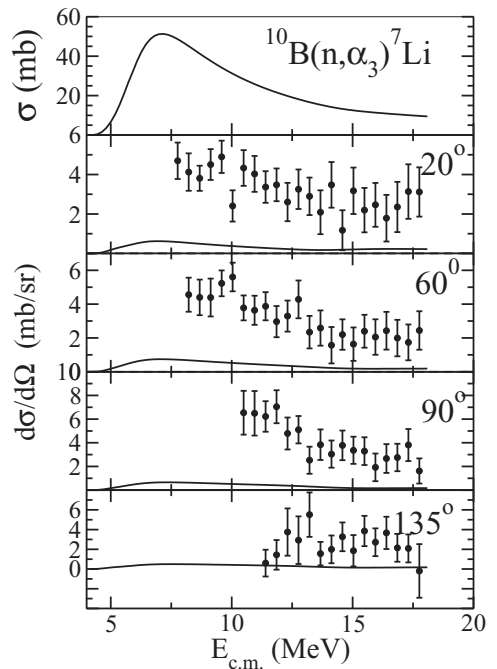


FIG. 13. *R*-matrix fits to the differential cross section for the $^{10}\text{B}(n, \alpha_3)$ reaction in the center of mass system. The results in the center of mass are labeled with the detector laboratory angle. The integrated cross section determined from the fit is shown in the uppermost panel.

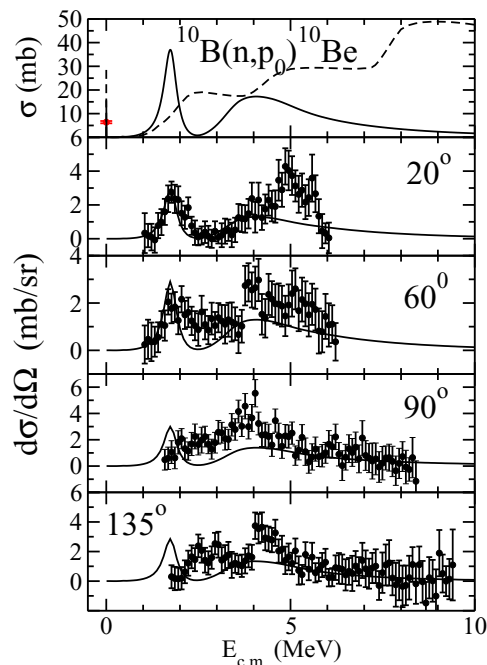


FIG. 14. R -matrix fit to the differential cross section of the $^{10}\text{B}(n, p_0)^{10}\text{Be}$ reaction in the center of mass system. All angles are shown with 100 keV binning and the integrated cross section determined from the fit is shown in the uppermost panel. The results from Lal *et al.* [10] (solid red circle) for thermal neutrons are shown in the angle integrated cross section (uppermost) plot (energy denoted by vertical dashed line in the top panel). The ENDF/B-VIII.0 evaluation [42] is shown as a dashed line. The data are labeled by the angle of the detector in the laboratory frame.

C. The $^{10}\text{B}(n, p_0)$ and $^{10}\text{B}(n, p_1)$ reactions

The current results for the $^{10}\text{B}(n, p_0)$ and $^{10}\text{B}(n, p_1)$ shown in Figs. 14 and 15 are limited due to the detector thickness. The current results at 8 MeV for $^{10}\text{B}(n, p_0)$ are ≈ 1 mb and consistent with the previous work [11].

An experiment by Davis *et al.* [4] found a resonance $E_n \sim 2.0$ MeV. In that experiment, a gridded proportional detector filled with boron trifluoride was used as both the target and detector. The separation of the reactions in this experiment was done using the pulse height. Thus, it was expected that that proton and triton channels could not be separated as the Q values of the two reactions are very similar.

Lal *et al.* [9,10] measured the thermal cross section $^{10}\text{B}(n, p_0)^{10}\text{Be}$ using a radiochemical technique resulting in a value of 6.4 ± 0.5 mb. Previous measurements of the angle integrated and angular distributions have been done at 14 MeV where the measured differential cross sections are less than 1 mb/sr for all of the observed proton groups [11].

The $^{10}\text{B}(n, p_1)^{10}\text{Be}(3.368)$ reaction has low cross sections. The data and R -matrix fit are shown for 90° and 135° in Fig. 15. The 20° differential cross section had background from the $\text{H}(n, n)\text{H}$ reaction. The 60° data have the bands from the $^{10}\text{B}(n, p_1)^{10}\text{Be}$ and $^{10}\text{B}(n, t_1)^{10}\text{Be}$ reactions overlapping. We do not report results for 20° and 60° for these reasons. The

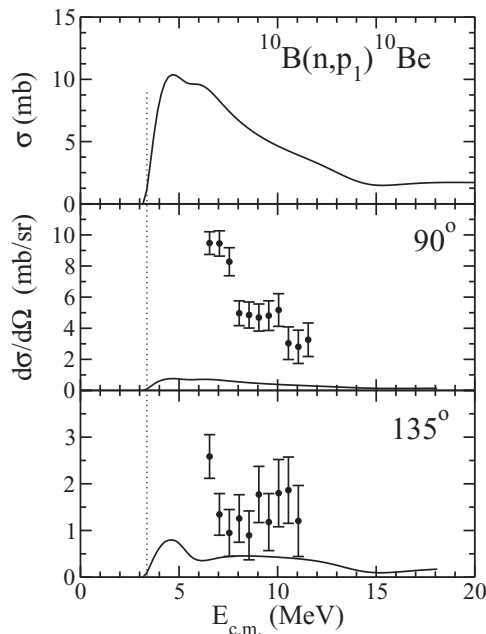


FIG. 15. R -matrix fit to the differential cross section of the $^{10}\text{B}(n, p_1)^{10}\text{Be}$ reaction in the center of mass system. All angles where the reaction could be identified above background are shown and the integrated cross section determined from the fit is shown in the uppermost panel. The threshold is shown as a dotted line. The data are labeled by the angle of the detector in the laboratory frame.

best fit was done with the known states. The fit is much below the data. We take this as evidence of additional states needed for describing the data.

D. The $^{10}\text{B}(n, t_0)$ and the $^{10}\text{B}(n, t_1)$ reactions

The results for the reactions $^{10}\text{B}(n, t_0)$ and $^{10}\text{B}(n, t_1)$ are shown in Fig. 16 and 17. There is some evidence in the differential cross section data for resonances near 4 and ≈ 7 MeV in the $^{10}\text{B}(n, t_0)$ reaction. There have been previous measurements of $^{10}\text{B}(n, t_0)$, and $^{10}\text{B}(n, t_1)$ reactions. An angular distribution was measured at 14.4 MeV [11,55] for the ground and first excited state. The ground and first excited state had maximum cross sections of 0.8 and 1.0 mb/sr, respectively. The current data (not shown at 14 MeV) are consistent with these measurements but the statistical errors on the current data are too large to make a meaningful comparison.

Measurements at thermal energies of the $^{10}\text{B}(n, t_0)$ reaction have been made by both radiochemical [26] and direct [25] methods, yielding 4.47 ± 0.15 mb and 7 ± 2 mb, respectively. The more accurate result of Clarke and Fleming [26] has been included in the data set for our R -matrix fit. Our final fit reproduces this value.

There has been a recent measurement of the $^{10}\text{B}(n, \alpha t)$ reaction using a twin gridded ionization detector [47,48]. The angular distributions of the α s or tritons were taken to be isotropic to unfold the measured pulse height spectra. The analysis of these data resulted in the determination of the $^{10}\text{B}(n, t + 2\alpha)$ reaction cross section. This result is the

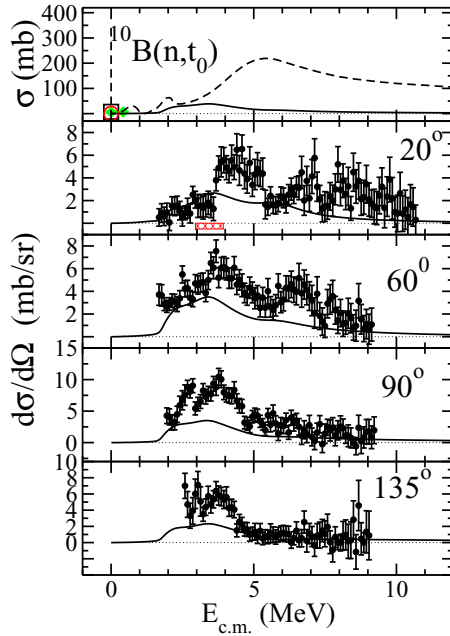


FIG. 16. R -matrix fit to the differential cross sections for the $^{10}\text{B}(n, t_0)$ reaction. The 20° differential cross sections have been taken from the runs with Xe/CO₂ gas. All angles are shown and the integrated cross section determined from the fit is shown in the uppermost panel. The area with possible contribution from the $\text{H}(n, n)\text{H}$ reaction is shown in red in the 20° plot. The measured cross sections at thermal energies (energy denoted by vertical dashed line in the top panel) are shown for Clarke and Fleming [26] (red open circle), and Kavanagh and Marley [25] (black open square) in the angle integrated cross section plot (uppermost). The low-energy cross section measurements of tritium production by Kornilov *et al.* [56] are shown (green diamonds). The ENDF/B-VIII.0 evaluation [42] is shown as a dashed line. The thermal cross section is shown with an axis offset at zero energy. The data are labeled by the angle of the detector in the laboratory frame.

sum of the $^{10}\text{B}(n, t_0)$ and the $^{10}\text{B}(n, \alpha_2)$ cross sections. Some information can be obtained from the ENDF evaluations for cross section channels of the $n + ^{10}\text{B}$ system. The estimated cross sections from ENDF/B-VII.0 and our work and (see the section on tritium production below) imply that the measured cross section is primarily from the $^{10}\text{B}(n, \alpha_2)$ reaction rather than $^{10}\text{B}(n, t_0)$.

E. The $^{10}\text{B}(n, d_0)$ reactions

The $^{10}\text{B}(n, d_0)$ reaction is weak with no clear resonances. The ENDF/B-VIII.0 evaluation [42] estimates the cross sections for the deuterium channel as larger than the proton channels. The threshold energies are shown in Table II for the population of the ground state and the first two excited states. Our current results are shown in Fig. 18. The $^{10}\text{B}(n, d_0)$ channel is only observed at 20° , 60° , and 90° with some background. We have tried to fit this reaction using the known states. No set of parameters gave any appreciable cross section for this channel. At 20° there is background which was ≈ 20 percent. The upper limit on the energy at 20° is due

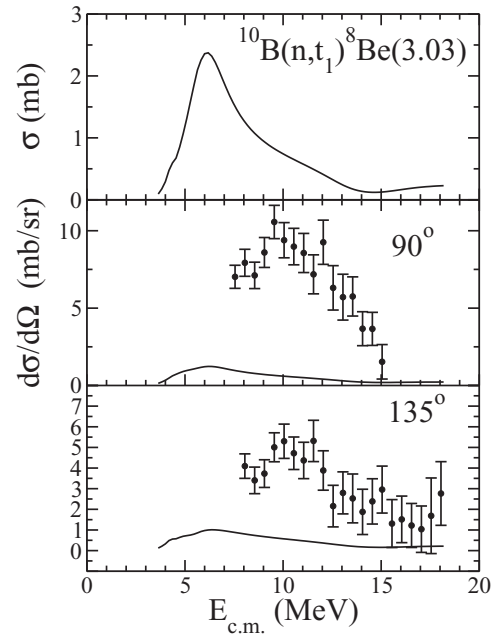


FIG. 17. R -matrix fits to the differential cross section the $^{10}\text{B}(n, t_1)$ reaction in the center of mass system. All angles are shown and the integrated cross section determined from the fit is shown in the uppermost panel. The data are labeled by the angle of the detector in the laboratory frame.

to a band of punch-through protons. The extracted cross section from both of the gas fillings resulted in the same cross section within error bars. This is despite an order of magnitude difference in the background. The $^{10}\text{B}(n, d_1)$ and $^{10}\text{B}(n, d_2)$ reactions could not be extracted due to both background and overlap with other channels.

Another way to obtain information on the $^{10}\text{B}(n, d_0)$ reaction would be to use the inverse reaction. The majority of the neutron flux for the $^9\text{Be}(d, n)$ reaction comes from neutron decay to the ground and excited states of ^{10}B . The studies of the $^9\text{Be}(d, n_0)$ reaction [14–21] provide data which can be used in an R -matrix fit.

V. R -MATRIX ANALYSIS

The R -matrix analysis was done for several reasons. A major reason was to estimate the integrated cross section from our differential cross section measurements. A second objective was to understand the nuclear structure of the observed states. Checking the measured cross section became important in the analysis of the $^{10}\text{B}(n, \alpha_2)$ and the $^{10}\text{B}(n, \alpha_3)$ reactions due to the contribution of the α s from breakup. A detailed evaluation of all of the channels of the $^{10}\text{B} + n$ system is beyond the capability of this work.

A. Inputs to R -matrix analysis

We have used the R -matrix code AZURE2 [57] in performing the fits to data. This code can perform the calculations in the R -matrix or level-matrix formalism, and this code has several features useful for this analysis such as the ability to

simultaneously calculate both the forward and inverse reactions. Angular distributions, excitation functions, and integral cross sections can be calculated. The data can be fitted using MINUIT2 fitting subroutine [58]. This fitting routine was implemented without restrictions on the value of the parameters. This unrestricted fitting often resulted in nonphysical results for the reduced width amplitudes. The Brune formalism [59] is also used when reporting the final results. The program allows input parameters as either widths or reduced width amplitudes. The fitting is done with the level energies and reduced width amplitudes. The reduced width amplitudes can be specified directly, by the partial widths, or the Asymptotic Normalization Coefficient (ANC).

The fitting with AZURE2 uses the cross section in the laboratory frame as inputs rather than to the angular distribution coefficients in the center of mass as had been done in earlier work in this compound nucleus [60]. The laboratory cross sections are converted to center-of-mass cross sections as an initial step in AZURE. Fitting the angular distributions with Legendre polynomials often leads to large correlations between the expansion coefficients. The fitting of data with AZURE2 where each angular distribution point is fitted leads to less bias in the fit.

The choice of the states to use for the R -matrix fit is important. Only the neutron channels have detailed angular distributions above 3 MeV incident neutron energy (≈ 13 MeV excitation energy). We have chosen to limit our fit to the previously known levels from [60] in the R -matrix fit. These states are compared to the the recent ENSDF evaluation in Table V. The reduced width parameters are also constrained by the Wigner limit as discussed below.

The R -matrix analysis by Sadowski *et al.* [60] fit the known neutron elastic and inelastic scattering data as well as the $^{10}\text{B}(n, \alpha_0)$ and $^{10}\text{B}(n, \alpha_1)$ data. It is important to note that the elastic neutron scattering and elastic α scattering have cross sections below what is expected using a hard sphere approximation. These lower cross sections can be obtained by placing large background states above the region of interest, an approach used by Sadowski *et al.* [60]. The elastic neutron scattering seems to be dominated by wide resonances above 4 MeV.

The reduced width amplitudes from Sadowski's work [60] were used as a starting point for fitting. The reported partial widths [60] were determined using the Ohio University R -matrix code. The energies of the resonances were determined using the single level approximation. This work was published before the development of the Brune formalism [59] which transforms the parameters to be at the actual excitation energy of the level. The Brune formalism [59] is used in AZURE2 R -matrix code as the standard way of reporting the fit parameters. There are 20 levels, 18 channels, and over 250 reduced width amplitudes in this parametrization. This leads to up to 2^{N-1} possible phases for each channel where N is the number of levels of a given spin and parity. While not all phase combinations are independent, this consideration requires care in fitting the data. Angular distributions are very useful in determining the contribution from individual resonances.

TABLE V. Energies of ^{11}B Levels. The known levels from the recent evaluation [29] are on the left and the levels used in the R -matrix fitting are on the right. *The 12.55 and 12.64 MeV states are discussed in Sec. VIE.

Ex. [29] (MeV)	J^π [29]	Γ_{total} [29]	Ex. (RM) [60] (MeV)	J^π
10.330(8)	$5/2^-$	112(10) keV		
10.602(4)	$7/2^+$	91(20) keV	10.6	$7/2^+$
(10.960(50))	$5/2^-$	≈ 4.5 MeV		
11.272(14)	$9/2^+$	110(20) keV		
11.450(17)	–	93(17) keV		
11.600(20)	$5/2^+$	180(20) keV	11.6	$5/2^+$
			11.8	$7/2^+$
11.893(13)	$5/2^-$	194(6) keV	11.9	$5/2^-$
12.04(13)	$7/2^+$	≈ 1 MeV		
12.554(13)*	$1/2^+$	205(20) keV		
12.63(40) [61]*	$(3/2^+)$	270^{+100}_{-70} keV		
12.917(11)	$1/2^-$	230(20) keV		
13.137(40)	$9/2^-$	426(40) keV	13.1	$9/2^-$
13.136	$(5/2^+, 7/2^+)$	363 keV	13.2	$5/2^+$
13.46(13) [62]	$1/2^+$	608(242) keV		
			13.7	$3/2^+$
			13.9	$5/2^-$
14.040(80)	$11/2^+$	0.5(2) MeV	14.0	$11/2^+$
14.340(20)	$5/2^+$	253(19) keV		
14.563(11)	–	≤ 30 keV		
14.55(7) [62]	$3/2^+$	475(80) keV		
14.74(9) [62]	$3/2^+$	830(145) keV		
15.290(25)	$(3/2, 5/2, 7/2)^+$	282(15) keV	15.2	$7/2^+$
			15.4	$5/2^-$
			15.6	$5/2^+$
			15.8	$9/2^-$
16.18(10) [62]	$(1/2, 3/2)^-$	≈ 60 keV		
16.432(10)	$T = (3/2)$	≤ 30 keV		
			16.5	$7/2^-$
			16.9	$5/2^-$
17.310	–	≈ 1 MeV		
17.500(30)	$T = (3/2)$	116(25) keV		
18.00(10)	$T = 3/2$	0.87(10) MeV		
			17.9	$7/2^-$
			18.1	$9/2^+$
18.370(50)	$(1/2, 3/2, 5/2)^+$	260(80) keV		
19.125(26)	$(7/2^-); 3/2$	115(25) keV		
			19.5	$5/2^-$
19.7	$(1/2^+)$	broad		
21.270(50)	$T = 3/2$	300(30) keV		
23.7	$(1/2, 3/2, 5/2)^+$			
26.5		broad		

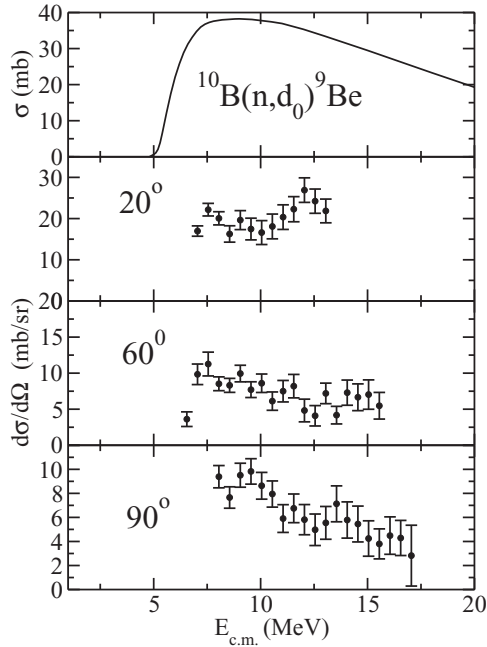


FIG. 18. The differential cross sections of the $^{10}\text{B}(n, d_0)$ reaction in the center of mass system. The data are labeled by the angle of the detector in the laboratory frame. The R -matrix fit is not shown but is very small. The upper panel shows the ENDF/B-VII.0 evaluated cross section for $^{10}\text{B}(n, d)$.

The available data on the channels in the $^{10}\text{B} + n$ system were collected. In the energy range of interest for this experiment several particle channels are of importance. Neutrons, protons, tritons, α s, and deuterons are the available decay channels. Thresholds for these reactions are shown in Table II. The available data useful for fitting were downloaded from the EXFOR data base at National Nuclear Data Center as discussed below.

There are considerable data covering the elastic and inelastic neutron scattering measurements. These have been well studied with detailed angular distributions over wide energy range. The elastic scattering from ^{10}B has been reported by several groups [5,63–67]. Measurements of the elastic and the weak inelastic channels also have been published [60,68–70].

The $^{10}\text{B}(n, \alpha)$ reaction has been studied in only a few experiments with good separation of the ground state and the first excited state, α_0 and α_1 [4,11,51,52]. The sum of the α_0 and α_1 cross sections has been measured [3,7,8,71]. Measurements using twin Frisch-grid ion chambers [7,44–49] have been used to extract the sum of the α_0 and α_1 cross sections. There has been a recent measurement by Jiang *et al.* [54] as was discussed above.

The ratio of the α_0 to α_1 cross section has also been measured [50,72,73] for the purpose of a neutron flux-standard determination. The work by Hamsch and Bax [50] with a twin gridded ion chamber resulted in both low-energy ratios of α_0 to α_1 and low-energy angular distributions.

The cross section of $^{10}\text{B}(n, \alpha_1)$ has been determined over the 5 keV to 4 MeV range by measurement of the γ ray from the first excited state in ^7Li [74,75]. These measurements are used in the R -matrix fits.

TABLE VI. The channel radii and Wigner limits for the channels in ^{11}B .

Channel	a_c (fm)	γ_{wc} (MeV)
neutrons	3.79	4.8
protons	3.79	4.8
deuterons	4.0	2.4
triton	4.11	1.8
α	4.20	1.4

There are also some data from elastic α scattering on ^7Li . There were several measurements of $^7\text{Li}(\alpha, \alpha)$ angle integrated and differential cross sections [61,76–81]. These measurements were previously fit to define the α channel. To obtain reasonable fits for the $3/2^-$ state at 6.5 MeV, Cusson [78] used a channel radius of ~ 6 fm. This is larger than what we have adopted (see Table VI). This state has been considered to be corresponding to the 0_2^+ state in ^{12}C which is also known as the Hoyle state [82–84]. The molecular states are discussed below. This variation in radius with excitation energy made data less useful in fitting the α data.

Data for the $^7\text{Li}(\alpha, n_0)$ reaction were very useful in understanding $\Gamma_{\alpha 0}$. There was however a question of the absolute normalization of the cross section. This was due to the nature of the lithium targets. Detailed angular distributions, and integral experimental data were available [52,85–91] for the $^7\text{Li}(\alpha, n_0)$ reaction at energies below the threshold of the first excited state.

Data from the $^9\text{Be}(d, n)$ reaction give little information on resonances in the deuteron cross section over the whole region of interest. Data from [14–17,92,93] show little resonance structure. The inverse angular distributions published were fit at low energies with a sum of even Legendre polynomials [93] and at higher energies by the optical model [15]. This does not allow a clear determination of the location of resonances and the reduced width amplitudes.

The $^{10}\text{Be}(p, \gamma)$ reaction has been measured at proton energies between 0.5 and 7 MeV [94]. The states populated by this reaction were $T = 3/2$ states in ^{11}B . The $T = 3/2$ states could be populated by neutrons incident on ^{10}B only through isospin mixing.

The reaction $p(^{10}\text{Be}, ^{10}\text{Be})p$ has been measured using a radioactive beam [62]. Their R -matrix fits to the data were used to deduce levels with spins and parities of $\frac{1}{2}^+$, $\frac{3}{2}^+$, $\frac{3}{2}^-$, and $(\frac{1}{2}, \frac{3}{2})^-$ in the excitation range of 13–16 MeV. States of these spins and parities were not found in previous studies of the $n + ^{10}\text{B}$ system. These states were tested but found to be of little importance to the $n + ^{10}\text{B}$ system due to the weak population of these low spin states in ^{11}B . Fits including these states showed no improvement in the R -matrix analysis of the current data. These states were excluded for the levels in the final R -matrix analysis.

The channel radii adopted for this work are given in Table VI. They are largely based on the previous R -matrix analysis of Sadowski *et al.* [60]. Systematic studies of the R -matrix fit to the channel radius were not attempted in this work.

One check on the R -matrix parameters is the Wigner limit. A limit on the reduced width, $\gamma_{\lambda c}^2$, has been given by Wigner [95–97]:

$$\gamma_{\lambda c}^2 \lesssim \frac{3\hbar^2}{2\mu_c a_c^2} = \gamma_{wc}^2, \quad (3)$$

where μ_c is the reduced mass of the channel and the channel radius is a_c . To compare the reduced widths to the Wigner limit it is useful to define the dimensionless reduced amplitude [98] $\theta_{\lambda c}$ as

$$\theta_{\lambda c} = \frac{\gamma_{\lambda c}^2}{\gamma_{wc}^2}. \quad (4)$$

Due to its dependence on the weakly constrained channel radius and other assumptions in its derivation, the Wigner limit is best understood as being an approximate limit. The Wigner limits for the ^{11}B compound nucleus are shown in Table VI. In our analysis, we considered the comparison to the Wigner limit as a method to discard fits when the reduced width amplitudes were more than a factor of two above the Wigner limit.

B. Results of R -matrix analysis

The R -matrix fits to our data and comparable data in the literature are discussed below. The parameters obtained from the R -matrix fit are given in Tables VII and the background states are given in Table VIII. The AZURE2 input file is included in the Supplemental Material [99]. It is important to note that the levels known from Sadowski *et al.* [60] have a maximum energy of 20 MeV which corresponds to a neutron energy of 9.5 MeV and a center of mass energy of 8.5 MeV.

The $^{10}\text{B}(n, \alpha_0)$ and $^{10}\text{B}(n, \alpha_1)$ reactions were not considered in the fitting as only the sum of both channels was observed at each angle. The contribution of the sum of both channels at the measured angle is shown in Fig. 9. The sum of these channels gives a poor constraint on the spin, parity and reduced width amplitude of the states. A very good fit can be made if the reduced width amplitudes were allowed to be much larger than the Wigner Limit. These fits were however discarded as physically incorrect.

The results for the $^{10}\text{B}(n, \alpha_2)$ channel and the R -matrix fits are shown in Figs. 12. We were able to obtain a reasonable fit with strongest contribution from levels with spin-parity of $7/2^+$ and $7/2^-$. The contribution of states with excitation above the known levels ($E_{c.m.} = 8.5$ MeV) describes the reaction up to 18 MeV in the center of mass. These reactions are important in the molecular states and $^{10}\text{B}(n, Xt)$ reactions as discussed below.

The results for the $^{10}\text{B}(n, \alpha_3)$ are shown in Fig. 13. This channel is expected to have the largest contribution from $5/2^+$, $5/2^-$, and $7/2^+$ states in ^{11}B . The result from our analysis shows that the current set of levels gives a result much lower than the observed cross section. Test fits showed that additional broad states above 20 MeV could explain the observed cross sections.

The observed resonance in the cross section reported by Davis [4] around $E_n \sim 2$ MeV is shown in Fig. 19. The work by Davis *et al.* [4] used a proportional chamber with the

TABLE VII. R -matrix Parameters using the known states in ^{11}B

J^π	E_x	c	ℓ	S	Γ or ANC	γ_c (MeV) ^{1/2}			
$7/2^+$	10.602	n_0	0	7/2	0.04	fm ^{1/2}	−0.05		
		α_0	3	3/2	1.0	eV	−0.15		
		α_1	3	1/2	9.0	keV	0.90		
		p_0	4	1/2	0.0001	fm ^{1/2}	0.05		
		t_0	4	1/2	0.003	fm ^{1/2}	0.05		
		$5/2^+$	11.605	n_0	0	5/2	250.0	keV	0.70
n_0	2			5/2	5.0	eV	0.10		
n_0	2			7/2	240.0	eV	0.70		
α_0	1			3/2	5.0	keV	−0.05		
α_1	3			1/2	20.0	keV	0.40		
p_0	2			1/2	500.0	meV	0.05		
t_0	2			1/2	2.0	eV	0.06		
$7/2^+$	11.8			n_0	0	7/2	650.0	keV	1.00
				α_0	3	3/2	7.0	keV	−0.15
				α_1	3	1/2	130.0	keV	0.90
		p_0	4	1/2	0.3	meV	0.05		
		t_0	4	1/2	9.0	meV	0.05		
		$5/2^-$	11.893	n_0	1	5/2	46.0	keV	0.5
n_0	1			7/2	46.0	keV	0.5		
α_0	2			3/2	3.0	keV	0.05		
α_1	2			1/2	4.0	keV	−0.07		
p_0	3			1/2	9.0	eV	0.5		
t_0	3			1/2	5.0	eV	0.1		
$9/2^-$	13.1	n_0	1	7/2	120.0	keV	0.44		
		α_0	4	3/2	160.0	keV	0.9		
		α_1	4	1/2	29.0	keV	0.5		
		p_0	5	1/2	8.0	meV	0.1		
		t_0	5	1/2	80.0	eV	−0.8		
		$5/2^+$	13.2	n_0	0	5/2	300.0	keV	0.45
n_1	2			1/2	20.0	keV	0.7		
n_1	2			3/2	20.0	keV	0.7		
α_0	1			3/2	30.0	keV	0.1		
α_1	3			1/2	7.0	keV	−0.1		
p_0	2			1/2	30.0	keV	0.65		
t_0	2			1/2	1.0	keV	0.05		
$3/2^+$	13.7			n_0	2	5/2	160.0	keV	0.9
				n_0	2	7/2	160.0	keV	0.9
				n_1	0	3/2	167.0	keV	0.38

TABLE VII. (*Continued.*)

J^π	E_x	c	ℓ	S	Γ or ANC	γ_c (MeV) ^{1/2}			
5/2 ⁻	13.9	α_0	1	3/2	167.0	keV	0.23		
		α_1	1	1/2	330.0	keV	0.35		
		α_2	3	7/2	17.0	meV	0.1		
		p_0	2	1/2	1.2	keV	0.1		
		t_0	2	1/2	170.0	keV	0.5		
		n_0	1	5/2	1200.0	keV	1.0		
		n_0	1	7/2	12.0	keV	0.1		
		n_1	1	3/2	380.0	keV	0.7		
		α_0	2	3/2	100.0	keV	0.2		
		α_1	2	1/2	100.0	keV	0.2		
11/2 ⁺	14.0	α_2	2	7/2	40.0	eV	-0.2		
		p_0	3	1/2	2.0	keV	0.4		
		t_0	3	1/2	2.0	keV	0.1		
		t_1	1	3/2	1.0	keV	0.03		
		n_0	2	7/2	500.0	keV	1.4		
		α_0	5	3/2	30.0	keV	0.6		
		α_1	5	1/2	6.0	keV	0.4		
		α_2	5	7/2	0.1	meV	0.05		
		7/2 ⁺	15.2	n_0	2	5/2	300.0	keV	1.0
				n_0	0	7/2	1100.0	keV	1.0
n_0	2			7/2	50.0	keV	0.4		
n_1	2			3/2	50.0	keV	-0.5		
n_3	2			3/2	50.0	keV	0.9		
n_4	2			3/2	250.0	eV	1.0		
n_4	2			5/2	250.0	eV	1.0		
α_0	3			3/2	23.0	keV	0.15		
α_1	3			1/2	46.0	keV	-0.2		
α_2	1			7/2	420.0	keV	1.0		
5/2 ⁺	15.6	α_3	1	5/2	530.0	keV	0.02		
		p_0	4	1/2	1.0	keV	0.9		
		p_1	2	3/2	670.0	eV	0.7		
		p_1	2	5/2	260.0	eV	0.4		
		t_1	2	3/2	55.0	eV	-0.05		
		t_1	2	5/2	870.0	eV	-0.2		
		n_0	0	5/2	1.3	MeV	1.		
		n_1	2	1/2	70.0	keV	0.5		
		n_1	2	3/2	70.0	keV	0.5		
		n_2	2	1/2	9.0	keV	0.25		
5/2 ⁻	16.9	n_3	2	1/2	4.0	keV	0.2		
		n_3	2	3/2	4.0	keV	0.2		
		n_4	2	3/2	370.0	eV	0.25		

TABLE VII. (*Continued.*)

J^π	E_x	c	ℓ	S	Γ or ANC	γ_c (MeV) ^{1/2}	
9/2 ⁻	15.8	n_4	0	5/2	30.0	keV	0.25
		n_4	2	5/2	370.0	eV	-0.25
		α_0	3	3/2	29.0	keV	0.15
		α_1	3	1/2	300.0	keV	0.5
		α_2	1	7/2	128.0	keV	0.4
		α_3	1	5/2	52.0	eV	-0.8
		p_0	2	1/2	620.0	keV	1.5
		p_1	0	5/2	270.0	keV	-0.9
		t_0	2	1/2	900.0	keV	-0.9
		t_1	0	5/2	7.0	keV	0.1
7/2 ⁻	16.5	n_0	1	7/2	8.0	keV	0.1
		n_1	3	3/2	5.0	keV	0.4
		n_4	3	3/2	30.0	eV	0.4
		n_4	3	5/2	60.0	eV	0.55
		α_0	4	3/2	5.0	keV	0.1
		α_1	4	1/2	10.0	keV	0.15
		α_2	2	7/2	280.0	keV	1.0
		α_3	2	5/2	45.0	eV	-0.5
		p_1	3	3/2	250.0	eV	-0.9
		p_1	3	5/2	200.0	eV	-0.8
5/2 ⁻	16.9	t_1	3	3/2	16.0	keV	-1.2
		t_1	3	5/2	12.0	keV	1.0
		n_0	1	5/2	1.3	MeV	1.0
		n_0	1	7/2	1.3	MeV	1.0
		n_1	3	1/2	120	keV	-1.24
		n_1	3	3/2	120	keV	-1.24
		n_2	3	1/2	2	keV	0.25
		n_3	3	1/2	4.0	keV	0.4
		n_3	3	3/2	4.0	keV	0.4
		n_4	1	5/2	240.0	keV	0.74
5/2 ⁻	16.9	α_2	0	7/2	1.7	MeV	1.0
		α_3	2	5/2	3.0	keV	-0.3
		p_1	1	5/2	80.0	keV	-0.5
		t_1	1	5/2	240.0	keV	0.5
		d_0	4	3/2	600.0	keV	0.5
		n_0	1	5/2	70.0	eV	-0.25
		n_0	1	7/2	700	eV	-0.25
		n_1	3	3/2	15.0	keV	0.4
		n_2	3	1/2	37.0	keV	1.0
		n_3	1	3/2	24.0	keV	-0.18
5/2 ⁻	16.9	n_4	1	3/2	110.0	keV	-0.5
		n_4	1	5/2	110.0	keV	-0.5

TABLE VII. (Continued.)

J^π	E_x	c	ℓ	S	Γ or ANC	γ_c (MeV) ^{1/2}	
		α_1	2	1/2	160.0	eV	-0.009
		α_2	2	7/2	730.0	eV	1.0
		α_3	0	5/2	80.0	eV	0.4
		p_0	3	1/2	80.0	eV	1.0
		p_1	1	3/2	90.0	keV	-0.5
		p_1	1	5/2	90.0	keV	-0.5
		t_0	3	1/2	190.0	keV	0.5
		t_1	1	3/2	590.0	keV	0.8
		t_1	1	5/2	590.0	keV	0.8
		d_0	2	3/2	20.0	keV	1.0
9/2 ⁻	17.8						
		n_0	1	7/2	290.0	keV	-0.5
		n_1	3	3/2	180.0	keV	-1.2
		n_3	3	3/2	85.0	keV	-1.3
		n_4	3	3/2	4.0	keV	0.50
		n_4	3	5/2	4.0	keV	0.5
		n_5	1	7/2	360.0	keV	1.0
		α_0	4	3/2	11.0	keV	0.1
		α_1	4	1/2	10.0	keV	0.1
		α_2	2	7/2	1.7	MeV	-1.3
		α_3	2	5/2	1.8	keV	0.08
		p_1	3	3/2	130.0	eV	-0.1
		p_1	3	5/2	8.0	keV	-0.8
		t_1	3	3/2	280.0	keV	1.1
		t_1	3	5/2	1.0	keV	0.07
		d_0	4	3/2	870.0	meV	-0.04
7/2 ⁻	17.9						
		n_0	1	5/2	970.0	keV	-1.0
		n_0	1	7/2	970.0	keV	-1.0
		n_1	3	1/2	77.0	keV	0.9
		n_1	3	3/2	77.0	keV	0.9
		n_2	3	1/2	39.0	keV	0.8
		n_3	3	1/2	783.0	eV	0.13
		n_3	3	3/2	783.0	eV	0.13
		n_4	1	5/2	330.0	keV	0.80
		n_5	1	5/2	80.0	keV	0.5
		n_5	1	7/2	80.0	keV	0.5
		α_2	0	7/2	1.5	MeV	-1.0
		α_3	2	5/2	300.0	keV	1.0
		p_0	3	1/2	4.0	keV	-0.2
		p_1	3	3/2	7.0	keV	0.75
		p_1	1	5/2	240.0	keV	0.75
		t_0	3	1/2	800.0	keV	1.0
		t_1	3	3/2	200.0	keV	1.0
		t_1	1	5/2	400.0	keV	0.6

TABLE VII. (Continued.)

J^π	E_x	c	ℓ	S	Γ or ANC	γ_c (MeV) ^{1/2}	
		t_1	3	5/2	200.0	keV	1.0
		d_0	4	3/2	2.0	eV	0.05
9/2 ⁺	18.1						
		n_0	2	5/2	200.0	keV	0.5
		n_0	2	7/2	200.0	keV	0.5
		n_4	2	5/2	30.0	keV	0.4
		n_5	2	5/2	80.0	keV	0.9
		n_5	2	7/2	80.0	keV	0.9
		α_2	1	7/2	1.7	MeV	0.9
		α_3	3	5/2	6.0	keV	-0.2
		p_0	4	1/2	300.0	eV	0.12
		p_1	2	5/2	100.0	keV	-0.75
		t_0	4	1/2	7.0	keV	-0.4
		t_1	2	5/2	900.0	keV	0.9
		d_0	3	3/2	30.0	keV	1.0
5/2 ⁻	19.5						
		n_0	1	5/2	670.0	keV	0.5
		n_0	1	7/2	670.0	keV	0.5
		n_4	1	3/2	360.0	keV	-0.5
		n_4	1	5/2	360.0	keV	-0.45
		α_2	2	7/2	7.0	MeV	-0.5
		α_3	0	5/2	3.2	MeV	-1.0
		p_0	3	1/2	36.0	keV	0.3
		p_1	1	3/2	62.0	keV	-0.2
		p_1	1	5/2	130.0	keV	-0.3
		t_0	3	1/2	430.0	keV	0.4
		t_1	1	3/2	1500.0	keV	0.7
		t_1	3	3/2	12.0	keV	0.1
		t_1	1	5/2	446.0	keV	-0.4
		t_1	3	5/2	12.0	keV	0.1
		d_0	2	3/2	10.0	keV	0.1

identification of the particle only by the Q value. Since the Q values for the $^{10}\text{B}(n, p_0)^{10}\text{Be}$ and $^{10}\text{B}(n, t_0)^8\text{Be}$ reaction are very close, the particle observed could not be identified. This was pointed out by Davis [4]. This result has been taken as contribution only to $^{10}\text{B}(n, t_0)^8\text{Be}$ reaction in the ENDF/B-VIII.0 [42] evaluation. The fit of the current data for the $^{10}\text{B}(n, p_0)^{10}\text{Be}$ reaction was found to well describe this resonance. There is some evidence in the R -matrix fit for additional state(s) above 4 MeV.

This 2 MeV resonance energy corresponds to an excitation energy of 13.19 MeV where a $5/2^+$ state was previously known as shown in Table V. The $^{10}\text{B}(n, t_0)^8\text{Be}$ reaction has data around 2 MeV at 20° and 60° degrees. There is little evidence of a resonance at this energy, but the $^{10}\text{B}(n, t_0)^8\text{Be}$

TABLE VIII. *R*-matrix Background States

J^π	E_x	c	ℓ	S	Γ or ANC	γ_c (MeV) ^{1/2}	
3/2 ⁻	25.1	n_0	1	5/2	11.5	MeV	1.5
		α_0	0	3/2	24.0	MeV	1.5
9/2 ⁺	25.2	n_0	2	5/2	3.8	MeV	1.0
9/2 ⁻	25.4	n_0	1	7/2	5.2	MeV	1.0
5/2 ⁺	26.2	n_0	0	5/2	24.0	MeV	2.0
		α_2	1	7/2	9.0	MeV	1.0
5/2 ⁻	26.3	n_0	1	7/2	5.5	MeV	1.0
7/2 ⁻	26.3	n_0	1	5/2	5.5	MeV	1.0
		n_0	0	7/2	6.1	MeV	1.0
9/2 ⁺	26.7	n_0	2	7/2	4.3	MeV	1.0

reaction has some broad strength above this region. A plot with 100 keV bins for this data near this resonance is shown in Fig. 19. The 5/2⁺ state at 13.19 MeV is limited to only weak contributions from α and triton channels in the *R*-matrix fit to this resonance.

An *R*-matrix fit can reproduce the thermal neutron cross section for the charged-particle channels. This fit is primarily dependent on the reduced width amplitudes of the 5/2⁺ state at 11.60 MeV for the ¹¹B for the ¹⁰B(*n*, *t*)⁸Be(*g.s.*) and ¹⁰B(*n*, *p*)¹⁰Be(*g.s.*) reactions. The reactions ¹⁰B(*n*, α_0)⁷Li(*g.s.*) and ¹⁰B(*n*, α_1)⁷Li(0.478) are more sensitive to the 7/2⁺ states at 10.602 and 12.040 MeV in ¹¹B.

For both the *p*₀ and *t*₀ channels the *R*-matrix fit is lower than the experiment above $E_n = 3$ MeV. Population of ¹⁰B(*n*, *p*)¹⁰Be and ¹⁰B(*n*, *t*)⁸Be are through a 5/2⁺ state. This is with an entrance $\ell = 0$ for the neutron and a $\ell = 2$ channel for the outgoing protons or tritons.

A fit with reasonable parameters for the ¹⁰B(*n*, *p*)¹⁰Be reaction below 3 MeV may be obtained using the known levels from Sadowski *et al.* [60]. The state at 13.2 MeV was previously assumed to be a 5/2⁺ state in the fit by Sadowski *et al.* [60]. A fit using the known 5/2⁻ states contributed less than 5% of the cross section in this region. A 3/2⁻ state was tested in this region but a single resonance did not result in a large enough cross section with reduced width amplitudes of up to 1.0 MeV^{1/2} for both the entrance and exit channels.

Both the ¹⁰B(*n*, *p*₁), and the ¹⁰B(*n*, *t*₁) reactions go to the 2⁺ first excited states of ¹⁰Be and ⁸Be respectively. The states in ¹¹B expected to contribute to these reactions have spin-

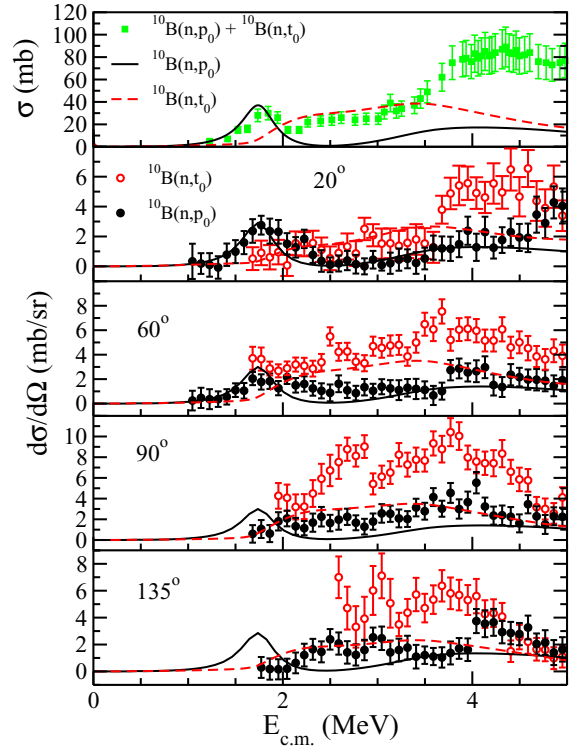


FIG. 19. A comparison of the ¹⁰B(*n*, *p*₀)¹⁰Be reaction data (black filled circles) and its *R*-matrix fit (solid black lines) and the ¹⁰B(*n*, *t*₀)⁸Be reaction data (red empty circles) and its *R*-matrix fit (red dashed lines) below 4 MeV. The sum of the cross sections for the ¹⁰B(*n*, *p*₀)¹⁰Be and ¹⁰B(*n*, *t*₀)⁸Be reactions from Davis *et al.* [4] are shown in the top panel as green points. The integrated cross section from the *R*-matrix fit are also shown in the top panel.

parities of 5/2⁺, 7/2⁺, and 5/2⁻. Neutron elastic and inelastic scattering should populate these states. We attempted to do an *R*-matrix fit to the data with the known states. A difficulty is that most of the data is above neutron energy of 8.3 MeV which is equivalent to the highest energy known state in ¹¹B.

For the ¹⁰B(*n*, *d*)⁹Be reaction, no combination of realistic parameters gave over a 1 mb cross section using the known states. Most of the data for ¹⁰B(*n*, *d*) reaction was above 6 MeV where contribution of states not included in the analysis are important.

The *R*-matrix analysis of the current and previous data allows an estimate of the angle integrated cross section for each reaction. A summary of the *estimated* cross sections along with the ENDF/B-VIII.0 [42] for previously measured channels is shown in Fig. 20.

The *R*-matrix fits may allow an understanding of the reactions important in the production of tritium in ¹⁰B by neutrons. The angle integrated cross section for the reactions leading to the break up to two α s and a triton has been measured in several ways. The earliest was by measurement of the tritium in boron-doped emulsions [22,23,100]. Radiochemical measurements of tritium production were carried out by several groups Clarke and Fleming [26], Suhaimi *et al.* [101], Qaim *et al.* [102], and Kornilov *et al.* [56]. A recent measurement was made using a twin gridded ionization

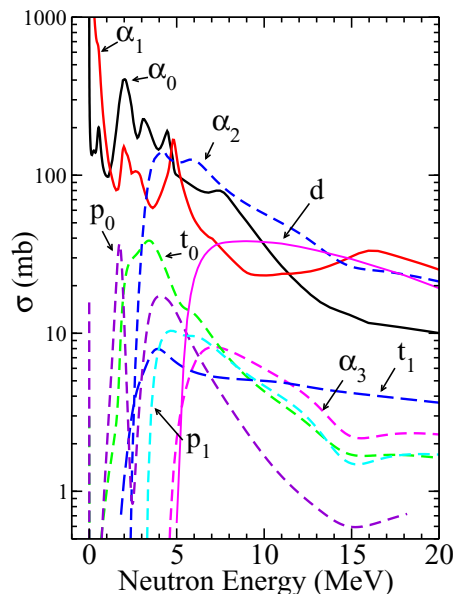


FIG. 20. A summary of the $^{10}\text{B}(n, Z)$ cross sections. The solid curves are from recent ENDF/B-VIII.0 evaluation [42] for the $^{10}\text{B}(n, \alpha_0)^7\text{Li}$ (black), $^{10}\text{B}(n, \alpha_1)^7\text{Li}$ (red), and $^{10}\text{B}(n, d)^9\text{Be}$ (solid magenta) reactions. The dashed curves are from the R -matrix fits in this work for the following reactions: $^{10}\text{B}(n, \alpha_2)^7\text{Li}$ (dashed blue), $^{10}\text{B}(n, \alpha_3)^7\text{Li}$ (dashed magenta), $^{10}\text{B}(n, p_0)^{10}\text{Be}$ (dashed purple), $^{10}\text{B}(n, p_1)^{10}\text{Be}$ (dashed light blue), $^{10}\text{B}(n, t_0)^8\text{Be}$ (dashed green), and $^{10}\text{B}(n, t_1)^8\text{Be}$ (long dashed blue).

chamber [47,48]. These data were used in the current ENDF/B-VIII.0 [42] evaluation. Our results for $^{10}\text{B}(n, p_0)$ shown in Fig. 19 is from Davis [4] where all of the cross section is assumed to be from the $^{10}\text{B}(n, t_0)$ reaction. The result from Davis *et al.* [4] includes the contribution from both protons and tritons. This was used in ENDF/B-VIII.0 [42]. Our results for $^{10}\text{B}(n, p_0)$ in Fig. 19 show that the measurement by Davis *et al.* [4] includes a substantial contribution from this reaction.

The two-body channels leading to tritium production are primarily $^{10}\text{B}(n, t_0)$, $^{10}\text{B}(n, t_1)$, $^{10}\text{B}(n, \alpha_2)$, and $^{10}\text{B}(n, \alpha_3)$. These reactions have been measured in this experiment. The tritium production accounted for by the R -matrix fit to the measured channels and the extrapolated values is shown in Fig. 21. The $^{10}\text{B}(n, t_1)$, $^{10}\text{B}(n, \alpha_2)$, and $^{10}\text{B}(n, \alpha_3)$ reactions have thresholds as shown in Table II. The minimum energy for observation of these reactions is higher than these values due to the target thickness, gas filling, and the detection thresholds in the experiment. The $^{10}\text{B}(n, \alpha_2)$ reaction dominates the production cross section at energies above 4 MeV. The current R -matrix fit shows that the sharp rise in the tritium production just above the threshold for $^{10}\text{B}(n, \alpha_2)$ can be accounted for by this reaction. The peak in the estimated cross section near threshold is weakly constrained by the measured cross section. The sum of these cross sections however does not account for the measured cross sections for tritium production above 6 MeV.

The additional tritium production above that predicted by these results above 5 MeV is likely due to several factors.

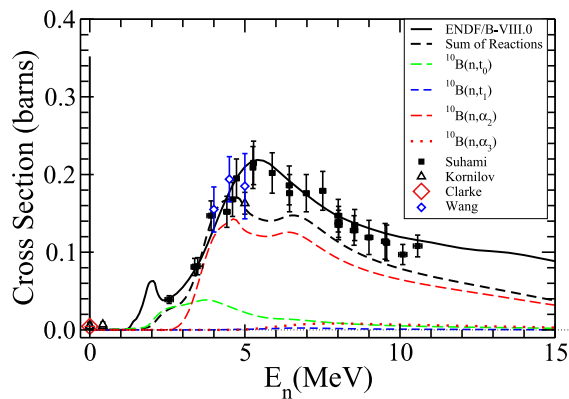


FIG. 21. Tritium production from ^{10}B irradiated with neutrons. Measurements are shown from Kornilov (open circle) [56], Suhami (solid squares) [101], Clarke (red diamond) [26], and Wang *et al.* [47] (blue triangle). The integrated cross sections obtained from the R -matrix fits to current data are shown for the $^{10}\text{B}(n, t_0)$ (dashed green line), $^{10}\text{B}(n, t_1)$ (dashed light blue dashed line), $^{10}\text{B}(n, \alpha_2)$ (solid red line), and the $^{10}\text{B}(n, \alpha_3)$ (dashed blue line). The ENDF/B-VIII.0 [42] evaluation for the production of tritium is shown as a solid black line.

An obvious problem is that the contribution of $^{10}\text{B}(n, \alpha_3)$ is greatly underestimated. This alone could explain most of the difference between experiment and the calculated sum of the reactions. A smaller contribution to this deficit is the omission of reactions which populate of higher energy states in ^8Be and ^7Li . An increase in the $^{10}\text{B}(n, t_1)$ cross section in energies above the $^{10}\text{B}(n, \alpha_2)$ reaction is not well constrained in the neutron energy range of 4–5 MeV. The R -matrix fit is also low for this reaction over most of the energy range.

VI. MOLECULAR AND CLUSTER STATES

The study of cluster and molecular states in nuclei is a active topic that has been recently reviewed [103,104]. There are two examples that have connection to our work.

One example is in the understanding of the molecular states. The classical example is the second 0^+ in ^{12}C , also known as the Hoyle state. This state was predicted by Hoyle to explain the abundance of carbon in the universe. This state can be considered to be a cluster of three α particles. The analogues of this state in the present work would be two neutrons coupled to two α s in ^{10}Be and a triton coupled to two α s in ^{11}B . Bands based on the molecular states have been observed in heavy ion reactions. The molecular states in ^{10}Be are observed, with a well established rotational bands. Calculations of molecular states in ^{11}B have been published by Descouvemont [105], Suhara and Kanada-En'yo [106], Kanada-En'yo and Suhara [107], and Zhou and Kimura [84].

A second example is proton decay of excited states in ^{11}B observed in the β^- decay of ^{11}Be [108]. These states would also need to have a large proton width to compete with the decay by α emission. The theory of enhancement of particle states near threshold has been advanced by Okołowicz *et al.* [109]. The coupling to the continuum may result in narrow resonances near threshold with a large proton spectroscopic factor.

There are a number of both positive and negative parity states predicted by Suhara and Kanada-En'yo [106]. The states with high α - or triton-reduced width amplitudes would be an indicator for cluster or molecular states. These cluster states are expected to have a larger radius than normally calculated by a simple $A^{1/3}$ dependence. Molecular states in ^{11}B can be thought of as two α s and a triton clusters. For configurations where these are linear this gives an estimate of a channel radius of 5 fm rather than the more traditional 4.1 fm channel radius for $t + ^8\text{Be}$ or a 4.2 fm channel radius for the $\alpha + ^7\text{Li}$.

The inelastic α scattering to the bound states in ^{11}B has been measured [82,83,110–112]. These experiments showed that the root mean square nuclear radius can be determined using the rainbow scattering and the Airy minimum versus energy. The $3/2^-$ state at 8.56 MeV needed a radius of 2.87 ± 0.12 fm, which is 0.6 fm larger than the ground state radius, to fit the measured angular distribution. This state is thought to be the lowest member of a molecular band built on the rotational band found in ^{10}Be coupled to a $p_{3/2}$ proton. This state is taken to be similar in structure to the 0_2^+ state in ^{12}C .

There have been resonant α scattering experiments completed to study states in ^{11}B by Yamaguchi *et al.* [61] and the mirror nucleus ^{11}C by Freer *et al.* [113]. These states were studied by α scattering from ^7Li and ^7Be beams at $\sim 180^\circ$ in the center of mass. They were searching for states with a high reduced width amplitude as a signature for cluster states. The $7/2^+$ state 10.60 MeV, the state 11.06 MeV, with likely spin-parity of $5/2^+$, and the $9/2^-$ state at 13.03 MeV were seen with large reduced width amplitudes in their analysis. The analog state in ^{11}C of the 10.60 state in ^{11}B was found with a similar α width by Freer [113].

The work by Soić [114] populated states in ^{11}B using the $^{14}\text{C}(^9\text{Be}, \alpha ^7\text{Li})^5\text{He}$ reaction. This reaction transfers a proton and a neutron onto a ^9Be nucleus. The decay of these states was measured by detecting the outgoing ^7Li and α in coincidence. Several states were identified as candidates for cluster states.

A transfer reaction experiment was also carried out with a radioactive ion beam of ^{12}B [115]. The targets of carbon and polyethylene were used. Detector arrays in the forward direction were used to detect the outgoing particles. Three sets of particles were correlated for ^{11}B to obtain information on the excitation energy of the levels. The $^7\text{Li} + \alpha$ pairs reconstruction showed a number of states. The $^{10}\text{Be} + p$ pairs gave peaks at ~ 13 and 14.34 MeV. Triple coincidences of two α s and a triton were also collected. The gate on the relative energy of the coincident α s was set to include only the final state decay of ^8Be . This showed several peaks above 15 MeV excitation energy.

The states and parameters needed to describe the low-energy elastic neutron scattering, the $^{10}\text{B}(n, \alpha_0)$, and the $^{10}\text{B}(n, \alpha_1)$ reactions were determined by the early workers on the $n + ^{10}\text{B}$ system [5,116]. The resonance states used in this fit are the $7/2^+$ state at 10.602 MeV, the $5/2^+$ state at 11.605 MeV, the $7/2^+$ state at 11.8 MeV, the $5/2^-$ state at 11.893 MeV, and the $9/2^-$ state at 13.1 MeV. The parameters of these states are dependent on the choice of the

method to account for the background from higher lying states [5,60,65,116]. The fitting of the low-energy cross sections has also been done as part of the neutron standards evaluation [1].

In this work, parameters to describe the low-energy $^{10}\text{B}(n, \alpha_0)$ and $^{10}\text{B}(n, \alpha_1)$ cross section were primarily from the results from Sadowski *et al.* [60]. We have used the results of our fitting of states above 13 MeV to better determine contribution to the well determined thermal cross sections. The $^{10}\text{B}(n, \alpha_0)$ and $^{10}\text{B}(n, \alpha_1)$ angular distributions are not available above ~ 2 MeV. The reduced width parameters of states were varied for the $7/2^+$ state at 10.602 MeV, the $5/2^+$ state at 11.605 MeV, and the $7/2^+$ state at 11.8 MeV to fit the thermal cross sections. This resulted in a tighter constraint on the reduced width amplitudes.

A wide range of channel radii for the α channel has been used for this system. The current work and Sadowski *et al.* [60] use $a_c = 4.2$ fm for α s as shown in Table VI. Earlier work used $a_c = 6$ fm for the α channels [78] and in fits to neutron and α channels [5,65,116]. The fits of α scattering by Yamaguchi *et al.* [61] used a a_c of 3.2 fm while the most recent work of Wiescher *et al.* [117] fitting the $^7\text{Li}(\alpha, \alpha)$, the $^7\text{Li}(\alpha, \alpha')$, and the $^7\text{Li}(\alpha, \gamma)$ reactions used 8 fm. The value of $\theta_{\lambda c}$ also depends on the square of the a_c as shown in Eqs. (3) and (4).

The value of $\theta_{\lambda c}$ of states observed in this experiment below 13.2 MeV are compared those found in searches for cluster states [61,83,114,117–119]. The correspondence of the resonance states from R -matrix analysis to the observed resonance by direct reactions becomes weak above 13.2 MeV.

A. The $7/2^+$ state at 10.602 MeV

The current results are similar to recent measurements. Our results for this state gives a $\theta_{\alpha_0} = 0.16$ and $\theta_{\alpha_1} = 0.58$. This is similar to previous R -matrix fitting of the $n + ^{10}\text{B}$ system [5,60]. The R -matrix fit of the data from Yamaguchi *et al.* [61] resulted in a $\theta_\alpha = 0.667$. A recent fit of the low-energy $^7\text{Li}(\alpha, \alpha)$, $^7\text{Li}(\alpha, \alpha')$, and $^7\text{Li}(\alpha, \gamma)$ yielded $\theta_\alpha = 0.26$ [117].

This state was observed as a doublet with the $5/2^-$ state at 10.330 MeV in the work by Danilov *et al.* [83]. Orbital angular momentum transfer contribution of $\ell = 5$, however the radius was unable to be extracted. This has been considered as the $7/2^+$ member of the $K = 3/2^+$ band [83]. A state was also seen at 10.55 MeV by Soić *et al.* [114].

The widths obtained by direct measurement of resonances differs from that found by R -matrix fitting. This width of this state has been evaluated as 91 ± 2 keV [29]. The widths for this state in R -matrix have been ~ 10 keV in both this work and Yamaguchi *et al.* [61]. A width of 31 keV was found in a R -matrix fits to the $^7\text{Li}(\alpha, \alpha)$, $^7\text{Li}(\alpha, \alpha')$, and $^7\text{Li}(\alpha, \gamma)$ reactions in recent work by Wiescher *et al.* [117]. Cusson [78] found the width of this state to be ~ 150 keV which was corrected for energy loss in the target to be $\sim 70 \pm 7$ keV. A larger correction for target thickness would bring the widths in line with those determined by R -matrix fitting.

To summarize, the large θ_{α_1} seen in this work is consistent with previous findings, leading to the identification of this

state as a candidate for a molecular state. This interpretation indicates that a large part of the wave function is based on an α coupled to the ${}^7\text{Li}$.

B. The $5/2^+$ state at 11.600 MeV

This state is primarily responsible for the $1/v$ behavior of the low-energy cross section for ${}^{10}\text{B}(n, p_0)$ and ${}^{10}\text{B}(n, t_0)$ reactions. The reduced width amplitudes for both the proton and triton are small. The results for α emission are $\theta_{\alpha 0} = 0.002$ and $\theta_{\alpha 1} = 0.16$. This is consistent with earlier R -matrix fits [5,60,65].

A state at this energy has also been seen in α scattering by Danilov *et al.* [83]. This was observed as a triplet with the 11.27- and 11.89-MeV states, which had unknown spin and parity. The angular distributions showed that there was a $5/2^+$ state as part of the multiplet. The radius deduced from α scattering was $r_{\text{rms}} = 2.17 \pm 0.39$ fm for $\ell = 1$ or $r_{\text{rms}} = 1.73 \pm 0.39$ fm for $\ell = 3$.

A state at this energy was seen in resonant α scattering by Yamaguchi *et al.* [61] and was assigned a tentative J^π of $7/2^-$ with $\theta_\alpha > 30$. This large value of θ_α may be due to the assumption of a spin-parity of $7/2^-$ instead of $5/2^+$.

This state has low values of $\theta_{\alpha 0}$ and $\theta_{\alpha 1}$. These results do not support the identification of this state as a molecular state.

C. The $7/2^+$ State at 11.8 MeV

A $7/2^+$ state at 12.04 MeV is known from earlier work [78] with $\Gamma \sim 1$ MeV. This is the closest state to the $7/2^+$ R -matrix resonance at 11.8 MeV. This state was seen in the ${}^7\text{Li}(\alpha, \alpha'){}^7\text{Li}$ reaction as part of a multiplet [78]. This state's width was assigned as 1 MeV to account for the observed cross section of the multiplet. In the ${}^{11}\text{B}(\alpha, \alpha)$ and ${}^{11}\text{B}(\alpha, \alpha')$ by Danilov *et al.* [83] the 11.8-MeV state is in a complex triplet with the 11.8-, 11.6-, and 11.27-MeV states. No radius was able to be determined.

The previous R -matrix fits [5,60,65,116] of the ${}^{10}\text{B}+n$ system for this state showed the importance of this state for both the explanation of the neutron and α cross sections at low energy. The results of these fits gave a value of $\theta_{\alpha 0}$ less than 0.1 for the ${}^{10}\text{B}(n, \alpha_0)$, and $\theta_{\alpha 1}$ of 0.8 for the ${}^{10}\text{B}(n, \alpha_1)$ channel.

This state has a large $\theta_{\alpha 1}$ and should be considered a candidate for a molecular state. The major portion of the wave function is expected to be an α coupled to the first excited state of ${}^7\text{Li}$.

D. The $5/2^-$ state at 11.893 MeV

The $5/2^-$ state is known [29] with a width of 196 ± 6 keV. Our and previous [5,60,65,116] R -matrix fits have the θ_α less than 0.01. This state was also seen weakly by Danilov *et al.* [83]. This state is not a good candidate for a cluster state due to the low value of θ_α .

E. The $9/2^-$ state at 13.137 MeV

This state has been observed in reactions looking for cluster states and in R -Matrix fits. The parameters of Sadowski *et al.* [60] were used for the neutron and α channels. This gave a $\theta_{\alpha 0} = 0.66$. The fit to the ${}^{10}\text{B}(n, t_0)$ data gave a $\theta_{t 0} = 0.44$.

Studies looking for cluster structures have seen this state in resonant α scattering [61] and decay following transfer reactions [114,115]. This has also been seen in ${}^7\text{Li}(\alpha, \alpha')$ by Cusson [78]. This state has been assigned as the $9/2^-$ member of the $K = 3/2^-$ band [83].

This state has both a large value of $\theta_{\alpha 0}$ and $\theta_{t 0}$. This suggests that the wave function has both a larger fraction of an α coupled to the ground state of ${}^7\text{Li}$ and a triton coupled to the ground state of ${}^8\text{Be}$. This supports the previous assignment of this state as a member of the $K = 3/2^-$ band.

F. States near 12.6 MeV

There is currently a question about the 12.55- and 12.63-MeV states. There are only a few experiments that have sufficient resolution to distinguish these states. Previous experiments used the reactions ${}^{10}\text{Be}(p, \gamma)$ [94], elastic, and inelastic scattering on ${}^7\text{Li}$ [61,77,78]. The ${}^{10}\text{Be}(p, \gamma)$ [94] populated a state at 12.55 ± 0.030 MeV. A state at 12.55 ± 0.02 MeV was also seen in inelastic α -particle scattering on ${}^7\text{Li}$ [78]. We consider these states to be the same. A state at 12.63 ± 0.04 MeV was seen in elastic α scattering on ${}^7\text{Li}$ at backward angles [61]. A measurement of ${}^7\text{Li}(\alpha, \alpha)$ at 150 degrees was made by Bohlen *et al.* [77] for center-of-mass energies below 3 MeV. Yamaguchi *et al.* [61] studied the same scattering but in inverse kinematics with a ${}^7\text{Li}$ beam on a helium target. They compared to the compiled data of Bohlen, which was assumed to be in center-of-mass rather than laboratory energies.

The properties of the state at 12.55 MeV are clear. The population of this state by the ${}^{10}\text{Be}(p, \gamma)$ reaction [94] shows the $T = 3/2$ character of the state. The results of Curtis [118] show that all of the $T = 3/2$ states are mixed and have α decay widths. This state is the lowest $T = 3/2$ state and has been assigned the spin-parity of $1/2^+$. This assignment has been confirmed in recent works to be the $T = 3/2$ by Barker [120,121] and Fortune [122].

The character of the 12.63 MeV state is not as clear. Yamaguchi [61] has limited the possible spin-parity assignments to $3/2^+$, $5/2^+$, $7/2^+$, and $9/2^+$. The $5/2^+$ and $7/2^+$ states are strongly populated by $\ell = 0$ transfer by neutrons in the $n + {}^{10}\text{B}$ system. The influence of a state at 12.62 MeV is not seen in any of the channels of this system. This makes the $5/2^+$ and $7/2^+$ spin-parity assignments unlikely.

The 12.55 MeV state, with a width of 150 keV, shows a fairly symmetric peak in inelastic α scattering on ${}^7\text{Li}$ at 60 degrees by Cusson [78]. Contribution from the 12.63 MeV state to this peak would be expected to produce a shoulder on the high-energy side of this peak. Several possible spin-parity were tried in the R -matrix analysis of Yamaguchi's data. Only a choice of $9/2^+$ gave a small width [61]. Yamaguchi reasoned that only a state with a small width would be compatible with the shape of this inelastic scattering peak. For this reason, they preferred a spin-parity of $9/2^+$ and a width of 42^{+9}_{-11} keV [61] for the 12.63-MeV state. These R -matrix fits also gave good results for the 13.1-MeV $9/2^-$ state. The dimensionless width for this state obtained by this R -matrix fit is the same as seen in this work and the elastic and inelastic

neutron scattering on ^{10}B by Sadowski *et al.* [60] as shown in Table IX.

The angle integrated cross section of the $^7\text{Li}(\alpha, \alpha')^7\text{Li}(0.478)$ reaction and the yield of the 0.478-MeV γ [78] show the 12.55-MeV peak with a tail on the high energy side where the contribution from the 12.63-MeV state would be expected. This tail shows that the width of the 12.63-MeV state is comparable to that of the 12.55-MeV state. A choice of $9/2^+$ for this state results in a width of of ~ 40 keV in the *R*-Matrix fits by Yamaguchi *et al.* [61]. This makes the spin-parity of the state most likely $3/2^+$ by elimination. A spin-parity of $3/2^+$ has been suggested a recent evaluation [27] and in the $^{11}\text{B} + \alpha$ scattering and by the results of Danilov *et al.* [83]. This would also require the 12.63-MeV resonance to be small at 60 degrees in the $^7\text{Li}(\alpha, \alpha')$ reaction.

Further investigations of elastic and inelastic α particle scattering from ^7Li with good resolution to measure the actual width and to determine the angular distribution at back angles would clarify the character to the 12.63-MeV state. The backwards angles are important for the resonant elastic α scattering experiments similar to those of Yamaguchi *et al.* [61].

G. Using the comparison of θ_p to θ_t as a test for cluster states

An additional check on the properties of excited states of ^{11}B may be possible. The ground state of ^{10}Be is expected to have little overlap with the known cluster or molecular states in ^{10}Be . Transfer reactions from the ground state of ^{10}Be do not populate the known molecular states in the heavier Beryllium isotopes [123,124]. The ^8Be nucleus can be described in part as states with a two α s cluster. A comparison of the spectroscopic factors or reduced width amplitudes of the $^{10}\text{B}(n, p_0)$ and the $^{10}\text{B}(n, t)$ reactions from a given state may allow identification of molecular or cluster states. The only clear proton resonance in our work was the $5/2^+$ state at 13.2 MeV. This state had a θ_{p0} of 0.09. This is large compared to the α and triton channels.

There is some additional information on states with proton widths. The decay of ^{11}B states by proton emission has been observed in other reactions. Two states with observed protons decay were seen in decay from excited states in ^{11}B [115]. There were also broad states. The $^7\text{Li}(\alpha, p)$ has shown broad states with excitation energies between 11.7 and 12.9 MeV [61].

Three states were able to be classified by this method. The states which had large triton cross sections were $9/2^-$ state at 13.1 MeV and the $3/2^+$ state at 13.7 MeV consistent with a cluster state. The $5/2^+$ state at 13.2 MeV has a large proton reduced width amplitude and should not be considered a cluster configuration.

1. States decaying by triton emission

We have observed several states which decay by triton emission. A large $\theta_{t0} = 0.5$ as seen for the 13.1-MeV $9/2^-$ state. There are also several states above this energy which have an large t_0 reduced width amplitude. The *R*-matrix states

TABLE IX. Collections of dimensionless reduced widths discussed in the Molecular and Cluster State section.

Resonance Energy	Spin parity	Channel Channel	$\theta_{\lambda c}$	Ref.
10.6	$7/2^+$	α_0	0.012	
			0.26	[117]
		α_1	0.19	[61]
			0.03	[60]
			0.03	[65]
			0.08	[5]
			0.41	
			0.2	[60]
			0.2	[65]
			0.59	[5]
11.6	$5/2^+$	α_0	0.001	
			0.06	[60]
		α_1	0.4	
			0.3	[60]
11.8	$7/2^+$	α_0	0.01	
			0.2	[60]
			0.0002	[65]
			0.006	[5]
		α_1	0.08	
			0.25	[60]
			0.04	[65]
			0.1	[5]
11.9	$7/2^+$	α_0	<0.001	
			0.03	[60]
		α_1	0.01	[65]
			0.003	
			0.04	[60]
			0.01	[65]
13.1	$9/2^-$	α_0	0.43	
			0.43	[61]
			0.43	[60]
			0.06	[65]
		α_1	0.13	
			0.13	[60]
			0.14	[65]
			0.004	
13.2	$5/2^+$	p_0	0.20	
			0.005	
		t_0	0.8	[60]
			0.02	[65]
			0.005	
			0.05	[60]
13.7	$3/2^+$	p_0	0.02	[65]
			0.02	
		t_0	0.02	
			0.008	
15.2	$7/2^+$	α_0	0.01	
			0.00.01	[60]
		α_1	0.05	[65]
			0.02	
			0.025	[60]
			0.008	[65]
16.5	$7/2^-$	α_2	0.5	
			0.5	
		α_3	0.5	
			0.05	

above 13.1 MeV have no known states corresponding to them.

Triton decay from ^{11}B excited states was observed in previous work. Soić [114,119] used the reactions $^9\text{Be}(^9\text{B}, ^7\text{Li} + \alpha)^5\text{He}$ and $^9\text{Be}(^9\text{B}, \alpha + \alpha)^5\text{He}$ reactions to study ^{11}B . In the analysis of the triple coincidence data evidence was found for decay by tritons of the 13.1 and 14.4 MeV states to the ground state of ^8Be . The 14.4- and 17.5-MeV states decay to $^8\text{Be}(3.03)$ and $^7\text{Li}(4.653)$ states. A broad distribution of states with triton decay with the constraint that the difference in energy between the two α s was small as expected from the decay of ^8Be were seen [115]. There were also some possible peaks identified. Seven states were identified as having triton decay by Curtis *et al.* [118].

2. States decaying to $^7\text{Li}(4.630)$

The $^{10}\text{B}(n, \alpha_2)^7\text{Li}$ channel is one of the dominant reactions at higher energies. The present data could not be fit with reduced width amplitudes of $\theta_{\alpha_2} \sim 1$. States seen in the α decay of excited states in ^{11}B to the 4.630-MeV state in ^7Li from were also observed to decay by triton to the ground and first excited state of ^8Be [115,119]. States seen in the α decay of excited ^{11}B to the 4.630-MeV state of ^7Li were also observed to triton decay to excited states in ^8Be . This gives some evidence that these states have cluster structure.

The α decay to the $^7\text{Li}(4.30)$ state has two clear resonances with large $\theta_{\lambda c}$. The $7/2^+$ resonance at 15.2 and the $7/2^+$ resonance at 15.5 both have $\theta_{\lambda c} \sim 0.7$ for the α decay to the 4.630-MeV state in ^7Li this is consistent width of a cluster state.

H. Summary of molecular and cluster state discussion

We have used the results of the R -matrix fit to infer partial widths of these states. A criteria of a large α $\theta_{\lambda c}$ has been

reviewed for the states observed in this work. The ratio triton to proton widths and the decay by α state to the particle unbound states of ^7Li has been presented. A summary of the results for the states observed in this work are shown in Table IX.

VII. SUMMARY

We have measured the differential cross sections for $^{10}\text{B}(n, Z)$ reactions at four angles for the $^{10}\text{B}(n, p_0)^{10}\text{Be}$, $^{10}\text{B}(n, t_0)^8\text{Be}$, $^{10}\text{B}(n, \alpha_2)^7\text{Li}$, and $^{10}\text{B}(n, \alpha_3)^7\text{Li}$ reactions between 2 and 20 MeV. The sum of the $^{10}\text{B}(n, \alpha_0)^7\text{Li}$ and $^{10}\text{B}(n, \alpha_1)^7\text{Li}$ differential cross sections has also been determined over this energy range. Partial angular distributions were measured for the $^{10}\text{B}(n, p_1)^{10}\text{Be}$, $^{10}\text{B}(n, t_1)^8\text{Be}$, and $^{10}\text{B}(n, d_0)^9\text{Be}$ reactions.

These new data are combined with literature data in an R -matrix analysis of the compound ^{11}B system. Candidates for cluster states are reviewed based on the R -matrix analysis.

ACKNOWLEDGMENTS

This work benefited from the use of the LANSCE accelerator facility and was performed under the auspices of the U.S. Department of Energy by Los Alamos National Security, LLC under Contract No. DE-AC52-06NA25396. The work at Ohio University has been supported by the U.S. Department of Energy, under Grants No. DE-FG52-09NA29455, No. DE-NA0001837, No. DE-NA0002905, No. DE-NA0003883, and No. DE-FG02-88ER40387. We thank Terry N. Taddeucci for his work in the conversion of the XSYS data to ascii format. We have had several discussions encouraging this work with G. M. Hale, M. W. Paris, and A. D. Carlson. John E. O'Donnell was involved in the actual experiment and has passed on during the course of this work.

-
- [1] A. D. Carlson, V. G. Pronyaev, R. Capote, G. M. Hale, Z.-P. Chen, I. Duran, F.-J. Hamsch, S. Kunieda, W. Mannhart, B. Marcinkevicius, R. O. Nelson, D. Neudecker, G. Noguere, M. Paris, S. P. Simakov, P. Schillebeeckx, D. L. Smith, X. Tao, A. Trkov, A. Wallner *et al.*, Evaluation of the neutron data standards, *Nucl. Data Sheets* **148**, 143 (2018), special Issue on Nuclear Reaction Data.
- [2] D. M. Gilliam, G. L. Greene, and G. P. Lamaze, Absolute neutron counting based on B-10 alpha-gamma-coincidence methods, *Nucl. Instrum. Methods Phys. Res., Sect. A* **284**, 220 (1989).
- [3] H. Bichsel and T. W. Bonner, Reactions $\text{Li}^7(\alpha, n)\text{B}^{10}$, $\text{Li}^7(\alpha, \alpha')\text{Li}^{7*}$, and $\text{B}^{10}(n, \alpha)\text{Li}^7$, *Phys. Rev.* **108**, 1025 (1957).
- [4] E. Davis, F. Gabbard, T. Bonner, and R. Bass, The disintegration of B^{10} and F^{19} by fast neutrons, *Nucl. Phys.* **27**, 448 (1961).
- [5] R. O. Lane, S. L. Hausladen, J. E. Monahan, A. J. Elwyn, F. P. Mooring, and A. Langsdorf Jr., ^{11}B States observed in the scattering of neutrons from ^{10}B and in the $^{10}\text{B}(n, \alpha)^7\text{Li}$ reaction, *Phys. Rev. C* **4**, 380 (1971).
- [6] A. M. Gagarski, G. V. Vaľsky, G. A. Petrov, Y. E. Loginov, V. E. Bunakov, I. S. Guseva, V. I. Petrova, and T. A. Zavarukhina, Triple correlation in the $^{10}\text{B}(n, \alpha\gamma)^7\text{Li}$ reaction, *JETP Lett.* **72**, 286 (2000).
- [7] G. Giorginis and V. Khryachkov, The cross-section of the $^{10}\text{B}(n, \alpha)^7\text{Li}$ reaction measured in the MeV energy range, *Nucl. Instrum. Methods Phys. Res., Sect. A* **562**, 737 (2006).
- [8] V. A. Khryachkov, I. P. Bondarenko, B. D. Kuzminov, N. N. Semenova, A. I. Sergachev, T. A. Ivanova, and G. Giorginis, (n, z) reactions cross section research at IPPE, *EPJ Web Conf.* **21**, 03005 (2012).
- [9] D. Lal, K. Nishiizumi, R. Reedy, M. Suter, and W. Wölfli, An accurate measurement of the $^{10}\text{B}(n, p)^{10}\text{Be}$ cross section at thermal energies, *Nucl. Phys. A* **468**, 189 (1987).
- [10] D. Lal, K. Nishiizumi, R. C. Reedy, M. Suter, and W. Wölfli, Errata, *Nucl. Phys. A* **481**, 834 (1988).
- [11] C. Sellem, J. P. Perroud, and J. F. Loude, Identification and spectrometry of charged particles produced in reactions induced by 14 MeV neutrons (II), *Nucl. Instrum. Methods* **128**, 495 (1975).

- [12] G. M. Ter-Akopian, P. N. Chuong, N. V. Yeregin, V. F. Strizhov, A. P. Kabachenko, and L. P. Chelnokov, $^{10}\text{Be}(p, n)$ reaction in the proton energy region < 2 MeV and a possible ultrasensitive method for ^{10}Be -analysis, *Nucl. Instrum. Methods Phys. Res., Sect. B* **17**, 393 (1986).
- [13] V. Valković, I. Člaus, P. Tomaš, and M. Cerineo, The reactions $^{10}\text{B}(n, t)$, $^7\text{Li}(n, t)$ and $^6\text{Li}(n, d)$ at 14.4 MeV, *Nucl. Phys. A* **98**, 305 (1967).
- [14] R. H. Siemssen, M. Cosack, and R. Felst, Reaction mechanism study of $\ell_p = 1$ stripping processes on nuclei of the 1p shell: (I) The reactions $\text{Be}^9(d, n)\text{B}^{10}$, $\text{B}^{10}(d, n)\text{C}^{11}$, and $\text{B}^{11}(d, n)\text{C}^{12}$, *Nucl. Phys.* **69**, 209 (1965).
- [15] A. A. Fife, G. C. Neilson, and W. K. Dawson, The excited states of ^{10}B , *Nucl. Phys. A* **91**, 164 (1967).
- [16] R. Bardes and G. E. Owen, Angular distributions of the $\text{Be}^9(d, n)\text{B}^{10}$ neutrons, *Phys. Rev.* **120**, 1369 (1960).
- [17] Y. S. Park, A. Niiler, and R. A. Lindgren, Spectroscopy of ^{10}B Levels from the $^9\text{Be}(d, n)^{10}\text{B}$ reaction, *Phys. Rev. C* **8**, 1557 (1973).
- [18] F. M. Baumann, G. Domogala, H. Freiesleben, H. J. Paul, S. Puhlfers, and H. Sohlbach, The $^9\text{Be}(d, n)^{10}\text{B}$ -reaction as intense neutron source with continuous energy spectrum, *Nucl. Instrum. Methods Phys. Res., Sect. A* **247**, 359 (1986).
- [19] M. A. Kayumov, S. S. Kayumov, S. P. Krekoten, A. M. Mukhamedzhanov, K. D. Razikov, K. Khamidova, and R. Yarmukhamedov, (d, n) and (p, n) reactions on light nuclei and their dispersion peripheral model analysis, *Yad. Fiz.* **48**, 629 (1988) [*Sov. J. Nucl. Phys.* **48**, 403 (1998)].
- [20] M. Febbraro, F. D. Becchetti, R. O. Torres-Isea, J. Riggins, C. C. Lawrence, J. J. Kolata, and A. M. Howard, (d, n) proton-transfer reactions on ^9Be , ^{11}B , ^{13}C , $^{14,15}\text{N}$, and ^{19}F and spectroscopic factors at $E_d = 16$ MeV, *Phys. Rev. C* **96**, 024613 (2017).
- [21] V. A. Vukolov, E. A. Koltypin, Y. D. Molchanov, and G. B. Yankov, Spectra of neutrons from the reactions $^6\text{Li}(d, n\alpha)^3\text{He}$ and $^9\text{Be}(d, n)^{10}\text{B}$ at deuteron energies up to 2.0 MeV, *Yad. Fiz.* **58**, 1539 (1995) [*Physics of Atomic Nuclei* **58**, 1453 (1995)].
- [22] J. Chadwick and M. Goldhaber, Disintegration by slow neutrons, *Nature (London)* **135**, 65 (1935).
- [23] H. J. Taylor, Disintegration of Boron by slow neutrons, *Proc. Phys. Soc.* **47**, 873 (1935).
- [24] V. Valković, Angular distribution of tritons from the reaction $\text{B}^{10} + n$ at 14.4 MeV, *Nucl. Phys.* **54**, 465 (1964).
- [25] R. W. Kavanagh and R. G. Marley, Thermal cross section for $^{10}\text{B}(n, t)2\alpha$, *Phys. Rev. C* **36**, 1194 (1987).
- [26] W. B. Clarke and R. F. Fleming, Thermal-neutron cross section for $^{10}\text{B}(n, t)2\alpha$ via $^3\text{He} - ^4\text{He}$ mass spectrometry, *Phys. Rev. C* **39**, 1633 (1989).
- [27] D. Tilley, C. Cheves, J. Godwin, G. Hale, H. Hofmann, J. Kelley, C. Sheu, and H. Weller, Energy levels of light nuclei $A = 5, 6, 7$, *Nucl. Phys. A* **708**, 3 (2002).
- [28] D. Tilley, J. Kelley, J. Godwin, D. Millener, J. Purcell, C. Sheu, and H. Weller, Energy levels of light nuclei $A = 8, 9, 10$, *Nucl. Phys. A* **745**, 155 (2004).
- [29] J. H. Kelley, E. Kwan, J. E. Purcell, C. G. Sheu, and H. R. Weller, Energy levels of light nuclei $A = 11$, *Nucl. Phys. A* **880**, 88 (2012).
- [30] P. W. Lisowski, C. D. Bowman, G. J. Russell, and S. A. Wender, The Los Alamos National Laboratory spallation neutron sources, *Nucl. Sci. Eng.* **106**, 208 (1990).
- [31] S. A. Wender, S. Balestrini, A. Brown, R. C. Haight, C. M. Laymon, T. M. Lee, P. W. Lisowski, W. McCorkle, R. O. Nelson, W. Parker, and N. W. Hill, A fission ionization detector for neutron flux measurements at a spallation source, *Nucl. Instrum. Methods Phys. Res., Sect. A* **336**, 226 (1993).
- [32] S. A. Wender, R. C. Haight, R. O. Nelson, C. M. Laymon, A. Brown, S. Balestrini, W. McCorkle, T. Lee, and N. W. Hill, *Fission Ionization Detector for Neutron Flux Measurements at a Spallation Source*, Tech. Rep. LAUR 90-399 (Los Alamos National Laboratory, Los Alamos, NM, 1993).
- [33] J. A. Stoner, ^{10}B isotopic analysis (private communication).
- [34] R. C. Haight, F. B. Bateman, S. M. Sterbenz, S. M. Grimes, O. A. Wasson, P. Maier-Komor, and H. Vonach, An update on $(n, \text{charged particle})$ research at WNR, *Fusion Eng. Des.* **37**, 73 (1997), Nuclear Data for Fusion Reactor Technology.
- [35] S. M. Grimes, C. E. Brient, F. C. Goeckner, F. B. Bateman, M. B. Chadwick, R. C. Haight, T. M. Lee, S. M. Sterbenz, P. G. Young, O. A. Wasson, and H. Vonach, The $^{59}\text{Co}(n, x\alpha)$ reaction from 5 to 50 MeV, *Nucl. Sci. Eng.* **124**, 271 (1996).
- [36] N. R. Yoder, XSYS, IUCF Data Acquisition Software, Indiana University Cyclotron Facility internal report (1991).
- [37] J. Ralston, The $^{10}\text{B}(n, \alpha)$ and $^{10}\text{B}(n, p)$ cross sections in the MeV energy range, Senior Thesis, Department of Physics and Astronomy, Ohio University, OH, 2011.
- [38] T. N. Massey, J. Ralston, S. M. Grimes, and R. C. Haight, $^{10}\text{B}(n, Z)$ measurements in the energy range 0.7 to 5.0 MeV, *Nucl. Data Sheets* **119**, 107 (2014), International Conference on Nuclear Data and for Science and Technology (2013).
- [39] W. T. Milner, *UPAK, the Oak Ridge Analysis Package*, Tech. Rep. (Oak Ridge National Laboratory, Tennessee, 1987).
- [40] J. F. Ziegler, M. D. Ziegler, and J. P. Biersack, SRIM - The stopping and range of ions in matter (2010), *Nucl. Inst. Meth. Phys. Res.* **268**, 1818 (2010).
- [41] M. B. Chadwick *et al.*, ENDF/B-VII.1 Nuclear data for science and technology: Cross sections, covariances, fission product yields and decay data, *Nuclear Data Sheets* **112**, 2887 (2011).
- [42] D. A. Brown *et al.*, ENDF/B-VIII.0: The 8th major release of the nuclear reaction data library with CIELO-project cross sections, New Standards and Thermal Scattering Data, *Nuclear Data Sheets* **148**, 1 (2018).
- [43] S. J. Friesenhahn, V. J. Orphan, A. D. Carlson, M. P. Fricke, and W. M. Lopez, Measurements of the ^6Li and ^{10}B partial cross sections from 1 to 1500 keV, in *Proceedings of the Conference on Nuclear Cross-Sections and Technology, Washington 1975* (National Bureau of Standards, Bethesda, MD, 1975), Vol. 1, p. 232.
- [44] G. Zhang, G. Tang, J. Chen, S. Zhang, Z. Shi, J. Yuan, Z. Chen, Y. M. Gledenov, M. Sedysheva, and G. Khuukhenkhuu, Differential cross-section measurement for the $^{10}\text{B}(n, \alpha)^7\text{Li}$ reaction, *Nucl. Sci. Eng.* **142**, 203 (2002).
- [45] G. Zhang, L. Guo, R. Cao, J. Zhang, and J. Chen, Cross-section measurement for the $^{10}\text{B}(n, \alpha)^7\text{Li}$ reaction at 4.0 and 5.0 MeV, *Appl. Radiat. Isot.* **66**, 1427 (2008).
- [46] G. H. Zhang, X. Liu, J. M. Liu, Z. H. Xue, H. Wu, and J. X. Chen, Measurement of cross sections for the $^{10}\text{B}(n, \alpha)^7\text{Li}$

- reaction at 4.0 and 5.0 MeV using an asymmetrical twin gridded ionization chamber, *Chin. Phys. Lett.* **28**, 082801 (2011).
- [47] Z. Wang, H. Bai, L. Zhang, H. Jiang, Y. Lu, J. Chen, G. Zhang, Y. M. Gledenov, M. V. Sedysheva, and G. Khuukhenkhuu, Cross section measurement for the $^{10}\text{B}(n, t2\alpha)$ three-body reaction at 4.0, 4.5, and 5.0 MeV. II. experimental setup and results, *Phys. Rev. C* **96**, 044621 (2017).
- [48] Z. Wang, H. Bai, L. Zhang, H. Jiang, Y. Lu, J. Chen, G. Zhang, Y. M. Gledenov, M. V. Sedysheva, and G. Khuukhenkhuu, Cross section measurement for the $^{10}\text{B}(n, t2\alpha)$ three-body reaction at 4.0, 4.5, and 5.0 MeV. I. Prediction of the experimental spectrum, *Phys. Rev. C* **96**, 044620 (2017).
- [49] G. Giorginis and V. Khriatchkov, The effect of particle leaking and its implications for measurements of the (n, α) reaction on light elements by using ionization chambers, *Nucl. Instrum. Methods Phys. Res., Sect. A* **538**, 550 (2005).
- [50] F. J. Hamsch and H. Bax, The standard branching ratio $^{10}\text{B}(n, \alpha_0)$ to $^{10}\text{B}(n, \alpha_1)$, *J. Nucl. Sci. Technol.* **39**, 1402 (2002).
- [51] F. J. Hamsch and I. Ruskov, The $^{10}\text{B}(n, \alpha_0)^7\text{Li}$ and $^{10}\text{B}(n, \alpha_1\gamma)^7\text{Li}$ alpha-particle angular distributions for $E_n < 1$ MeV, *Nucl. Sci. Eng.* **163**, 1 (2009).
- [52] R. M. Sealock, W. Hsiao-Yuan, and J. C. Overlay, $^7\text{Li}(\alpha, n)^{10}\text{B}$ differential cross-section measurements from threshold to $E_\alpha = 5.1$ MeV, *Nucl. Phys. A* **357**, 279 (1981).
- [53] G. Tang, G. Zhang, J. Chen, Z. Shi, J. Yuan, Z. Chen, Y. M. Gledenov, M. Sedysheva, and G. Khuukhenkhuu, *Angular Distribution and Cross Section Measurement for $^{10}\text{B}(n, \alpha)^7\text{Li}$ Reaction*, Tech. Rep. INDC(CPR)-053/L,P1 (Peking University, Institute of Heavy Ion Physics and MOE Key Laboratory of Heavy Ion Physics Beijing, China, 2001).
- [54] H. Jiang, W. Jiang, H. Bai, Z. Cui, G. Zhang, R. Fan, H. Yi, C. Ning, L. Zhou, J. Tang, Q. An, J. Bao, Y. Bao, P. Cao, H. Chen, Q. Chen, Y. Chen, Y. Chen, Z. Chen, C. Feng *et al.*, Measurements of differential and angle-integrated cross sections for the $^{10}\text{B}(n, \alpha)^7\text{Li}$ reaction in the neutron energy range from 1.0 eV to 2.5 MeV, *Chin. Phys. C* **43**, 124002 (2019).
- [55] V. Valković, G. Paić, I. Šlaus, P. Tomaš, and M. Cerineo, Reactions $^{48}\text{Ti}(n, d)^{47}\text{Sc}$, $^{16}\text{O}(n, d)^{15}\text{N}$, $^{19}\text{B}(n, d)^9\text{Be}$, and $^6\text{Li}(n, d)^5\text{He}$ at 14.4 MeV, *Phys. Rev.* **139**, B331 (1965).
- [56] N. Kornilov, A. Balitskij, V. Baryba, V. Druzhnin, A. Kagalenko, and A. Kharitonov, Investigation of the $^{10}\text{B}(n, t)$ reaction cross-section in the subthreshold energy region, *Yadernye Konstanty* **1**, 11 (1990).
- [57] R. E. Azuma, E. Uberseder, E. C. Simpson, C. R. Brune, H. Costantini, R. J. de Boer, J. Görres, M. Heil, P. J. LeBlanc, C. Ugalde, and M. Wiescher, Azure: An R-matrix code for nuclear astrophysics, *Phys. Rev. C* **81**, 045805 (2010).
- [58] F. James, *Minuit: Function Minimization and Error Analysis*, 94.1 ed., Tech. Rep. (CERN, Geneva, Switzerland, 1994).
- [59] C. R. Brune, Alternative parametrization of R-matrix theory, *Phys. Rev. C* **66**, 044611 (2002).
- [60] E. T. Sadowski, H. D. Knox, D. A. Resler, and R. O. Lane, Higher excitation levels of B^{11} via the $\text{B}^{10}(n, n)\text{B}^{10}$ and $\text{B}^{10}(n, n')\text{B}^{10*}$ (0.72, 1.74, 2.15, 3.59, 4.77 MeV) reactions, *Phys. Rev. C* **42**, 190 (1990).
- [61] H. Yamaguchi, T. Hashimoto, S. Hayakawa, D. N. Binh, D. Kahl, S. Kubono, Y. Wakabayashi, T. Kawabata, and T. Teranishi, α resonance structure in ^{11}B studied via resonant scattering of $^7\text{Li} + \alpha$, *Phys. Rev. C* **83**, 034306 (2011).
- [62] Y. D. Liu, H. W. Wang, Y. G. Ma, X. G. Cao, G. Q. Zhang, D. Q. Fang, M. Lyu, W. B. He, Z. T. Dai, C. Li, C. L. Zhou, S. Q. Ye, C. Tao, J. Wang, S. Kumar, J. L. Han, Y. Y. Yang, P. Ma, J. B. Ma, S. L. Jin *et al.*, New measurement of the excited states in ^{11}B via elastic resonance scattering of $^{10}\text{Be} + p$, *Phys. Rev. C* **91**, 044302 (2015).
- [63] J. M. Cox, H. D. Knox, R. O. Lane, and R. W. Finlay, Evidence for assignment of 14.0 MeV state in ^{11}B from $^{10}\text{B}(n, n)^{10}\text{B}$, *Nucl. Phys. A* **203**, 89 (1973).
- [64] J. H. Dave and C. R. Gould, Optical model analysis of scattering of 7- to 15-MeV neutrons from 1 - p shell nuclei, *Phys. Rev. C* **28**, 2212 (1983).
- [65] S. L. Hausladen, C. E. Nelson, and R. O. Lane, Structure study of ^{11}B from the scattering of neutrons from ^{10}B , *Nucl. Phys. A* **217**, 563 (1973).
- [66] H. D. Knox, R. M. White, and R. O. Lane, Differential elastic scattering cross-sections of ^{10}B for neutrons of 4 to 8 MeV energy, *Nucl. Sci. Eng.* **65**, 65 (1978).
- [67] H. B. Willard, J. K. Bair, and J. D. Kington, Elastic scattering angular distributions of fast neutrons on light nuclei, *Phys. Rev.* **98**, 669 (1955).
- [68] J. A. Cookson and J. G. Locke, Elastic and inelastic scattering of 9.72 MeV neutrons by ^{10}B and ^{11}B , *Nucl. Phys. A* **146**, 417 (1970).
- [69] S. G. Glendinning, S. El-Kadi, C. E. Nelson, R. S. Pedroni, F. O. Pursler, R. L. Walter, A. G. Beyerle, C. R. Gould, L. W. Seagondollar, and P. Thambidurai, Elastic and inelastic neutron cross sections for Boron-10 and Boron-11, *Nucl. Sci. Eng.* **80**, 256 (1982).
- [70] A. Takahashi, J. K. Oshima, M. Ueda, M. Fukazawa, Y. Yanagi, J. Miyaguchi, and K. Sumita, Measurements of double differential neutron emission cross sections for fusion reactor candidate elements, *J. Nucl. Sci. Technol.* **21**, 577 (1984).
- [71] B. Antolković, J. Hudomalj, B. Janko, G. Paić, and M. Turk, Measurement of the $^{10}\text{B}(n, \alpha)$ reaction at $E_n = 14.4$ MeV leading to stable and unstable levels of ^7Li , *Nucl. Phys. A* **139**, 10 (1969).
- [72] R. Bevilacqua, F. Hamsch, M. Vidali, I. Ruskov, and L. Lamia, $^{10}\text{B}(n, \alpha)^7\text{Li}$ and $^{10}\text{B}(n, \alpha_1\gamma)^7\text{Li}$ cross section data up to 3 MeV incident neutron energy, *EPJ Web Conf.* **146**, 11010 (2017).
- [73] W. M. Toney and A. W. Waltner, An investigation of the $^{10}\text{B}(n, \alpha)^7\text{Li}^*$, ^7Li reaction branching ratio, *Nucl. Phys.* **80**, 237 (1966).
- [74] R. A. Schrack, G. P. Lamaze, and O. A. Wasson, A measurement of the $^{10}\text{B}(n, \alpha\gamma)^7\text{Li}$ cross section in the keV energy region, *Nucl. Sci. Eng.* **68**, 189 (1978).
- [75] R. A. Schrack, O. A. Wasson, D. C. Larson, J. K. Dickens, and J. H. Todd, A Relative measurement of the $^{10}\text{B}(n, \alpha\gamma)^7\text{Li}$ cross-section between 0.2 and 4.0 MeV, *Nucl. Sci. Eng.* **114**, 352 (1993).
- [76] H. G. Bingham, K. W. Kemper, and N. R. Fletcher, Elastic scattering of ^4He from ^6Li and ^7Li at 12.0 to 18.5 MeV, *Nucl. Phys. A* **175**, 374 (1971).
- [77] H. Bohlen, N. Marquardt, W. Von Oertzen, and P. H. Gorodetzky, Nucleon exchange in the low-energy scattering of α -particles on ^6Li and ^7Li , *Nucl. Phys. A* **179**, 504 (1972).
- [78] R. Y. Cusson, Levels in ^{11}B from $^7\text{Li}(\alpha, \alpha')^7\text{Li}$ and $^7\text{Li}(\alpha, \alpha')^7\text{Li}'$ (0.48), *Nucl. Phys.* **86**, 481 (1966).

- [79] H. Kelleter, G. Hrehuss, and C. Mayer-Böricke, Investigations on the scattering of α particles on ${}^7\text{Li}$, *Nucl. Phys. A* **210**, 502 (1973).
- [80] J. P. Stoquert, N. Bendjaballah, H. Beaumevielle, C. Gérardin, and R. Seltz, Niveaux excités de ${}^{11}\text{B}$ observés dans la diffusion ${}^4\text{He} + {}^7\text{Li}$, *J. Phys. France* **40**, 813 (1979).
- [81] K. Rusek, P. D. Cathers, E. E. Bartosz, N. Keeley, K. W. Kemper, and F. Maréchal, Scattering of polarized ${}^7\text{Li}$ from ${}^4\text{He}$, *Phys. Rev. C* **67**, 014608 (2003).
- [82] A. N. Danilov, A. S. Demyanova, A. A. Ogloblin, S. V. Dmitriev, T. L. Belyaeva, S. A. Goncharov, Y. B. Gurov, V. A. Maslov, Y. G. Sobolev, W. Trzaska, S. V. Khlebnikov, N. Burtebaev, T. Zholdybayev, N. Saduyev, P. Heikkinen, R. Julin, and G. P. Tyurin, Cluster states in ${}^{11}\text{B}$, *EPJ Web of Conferences* **66**, 03007 (2014).
- [83] A. N. Danilov, A. S. Demyanova, S. V. Dmitriev, A. A. Ogloblin, T. L. Belyaeva, S. A. Goncharov, Y. B. Gurov, V. A. Maslov, Y. G. Sobolev, W. Trzaska, S. V. Khlebnikov, P. Heikkinen, R. Julin, G. P. Tyurin, N. Burtebaev, and T. Zholdybayev, Study of elastic and inelastic ${}^{11}\text{B} + \alpha$ scattering and search for cluster states of enlarged radius in ${}^{11}\text{B}$, *Phys. At. Nucl.* **78**, 777 (2015).
- [84] B. Zhou and M. Kimura, $2\alpha + t$ cluster structure in ${}^{11}\text{B}$, *Phys. Rev. C* **98**, 054323 (2018).
- [85] J. K. Bair and J. G. del Campo, Neutron yields from alpha-particle bombardment, *Nucl. Sci. Eng.* **71**, 18 (1979).
- [86] R. L. Macklin and J. H. Gibbons, Study of ${}^{10}\text{B}(n, \alpha){}^7\text{Li}$, ${}^7\text{Li}^*$ for $30 < E_n \text{ keV} < 500$, *Phys. Rev.* **165**, 1147 (1968).
- [87] M. K. Mehta, W. E. Hunt, H. S. Plendl, and R. H. Davis, A study of the $\text{Li}^6(\alpha, n)\text{B}^9$ and $\text{Li}^7(\alpha, n)\text{B}^{10}$ reactions, *Nucl. Phys.* **48**, 90 (1963).
- [88] M. D. Olson and R. W. Kavanagh, ${}^7\text{Li}(\alpha, n)$ cross section from threshold to 5.67 MeV, *Phys. Rev. C* **30**, 1375 (1984).
- [89] H. Tagziria and M. Looman, The ideal neutron energy spectrum of ${}^{241}\text{AmLi}(\alpha, n){}^{10}\text{B}$ sources, *Appl. Radiat. Isot.* **70**, 2395 (2012).
- [90] L. van der Zwan and K. W. Geiger, The ${}^7\text{Li}(\alpha, n){}^{10}\text{B}$ differential cross section for α -energies of up to 8 MeV, *Nucl. Phys. A* **180**, 615 (1972).
- [91] C. W. Wang, G. C. Kiang, L. L. Kiang, G. C. Jon, and E. K. Lin, The $\alpha + {}^7\text{Li}$ and $\alpha + {}^{12}\text{C}$ elastic scattering at $E_\alpha = 5$ and 6 MeV, *J. Phys. Soc. Jpn.* **51**, 3093 (1982).
- [92] S. G. Buccino and A. B. Smith, Levels in ${}^{10}\text{B}$ excited by the ${}^9\text{Be}(d, n)$ reaction, *Phys. Lett.* **19**, 234 (1965).
- [93] J. B. Garg, N. H. Gale, and J. M. Calvert, Neutron-gamma angular correlation studies from the reaction ${}^9\text{Be}(d, n\gamma){}^{10}\text{B}$, *Nucl. Phys.* **37**, 319 (1962).
- [94] D. R. Goosman, E. G. Adelberger, and K. A. Snover, $T = \frac{3}{2}$ levels in ${}^{11}\text{B}$ from the ${}^{10}\text{Be}(p, \gamma){}^{11}\text{B}$ reaction, *Phys. Rev. C* **1**, 123 (1970).
- [95] E. P. Wigner and L. Eisenbud, Higher angular momenta and long range interaction in resonance reactions, *Phys. Rev.* **72**, 29 (1947).
- [96] T. Teichmann and E. P. Wigner, Sum rules in the dispersion theory of nuclear reactions, *Phys. Rev.* **87**, 123 (1952).
- [97] C. B. Dover, C. Mahaux, and H. A. Weidenmüller, The single-particle limit for partial widths, *Nucl. Phys. A* **139**, 593 (1969).
- [98] M. H. Macfarlane and J. B. French, Stripping reactions and the structure of light and intermediate nuclei, *Rev. Mod. Phys.* **32**, 567 (1960).
- [99] See Supplemental Material at <http://link.aps.org/supplemental/10.1103/PhysRevC.105.054612> for AZURE2 input file in reduced width amplitude format.
- [100] G. M. Frye and J. H. Gammel, $\text{B}^{10}(n, t2\alpha)$ and $\text{B}^{10}(n, dn'2\alpha)$ Reactions for 6–20 MeV Neutrons, *Phys. Rev.* **103**, 328 (1956).
- [101] A. Suhaimi, R. Wölfle, S. M. Qaim, and G. Stöcklin, Measurement of ${}^{10}\text{B}(n)2\alpha$ reaction cross section in the energy range of 2.5 to 10.6 MeV: Diffusion of tritium in boron carbide, *Radiochim. Acta* **40**, 113 (1986).
- [102] S. M. Qaim, R. Wölfli, G. Stöcklin, M. Rahman, S. Sudar, and A. Suhaimi, Determination of (n , charged particle) reaction cross sections for FRT-relevant materials, in *Radiation Effects* (Gordon and Breach, New York, 1986), Vol. 92, p. 97.
- [103] M. Freer and A. C. Merchant, Developments in the study of nuclear clustering in light even-even nuclei, *J. Phys. G: Nucl. Part. Phys.* **23**, 261 (1997).
- [104] M. Freer, The clustered nucleus—Cluster structures in stable and unstable nuclei, *Rep. Prog. Phys.* **70**, 2149 (2007).
- [105] P. Descouvemont, Application of an extended cluster model to the ${}^8\text{Li}(\alpha, n){}^{11}\text{B}$ reaction, *Nucl. Phys. A* **596**, 285 (1996).
- [106] T. Suhara and Y. Kanada-En'yo, Cluster structures in ${}^{11}\text{B}$, *Phys. Rev. C* **85**, 054320 (2012).
- [107] Y. Kanada-En'yo and T. Suhara, $2\alpha + t$ cluster feature of the $3/2^-$ state in ${}^{11}\text{B}$, *Phys. Rev. C* **91**, 014316 (2015).
- [108] Y. Ayyad, B. Olaizola, W. Mittig, G. Potel, V. Zelevinsky, M. Horoi, S. Beceiro-Novo, M. Alcorta, C. Andreoiu, T. Ahn, M. Anholm, L. Atar, A. Babu, D. Bazin, N. Bernier, S. S. Bhattacharjee, M. Bowry, R. Caballero-Folch, M. Cortesi, C. Dalitz *et al.*, Direct Observation of Proton Emission in ${}^{11}\text{Be}$, *Phys. Rev. Lett.* **123**, 082501 (2019).
- [109] J. Okołowicz, M. Płoszajczak, and W. Nazarewicz, Convenient Location of a Near-Threshold Proton-Emitting Resonance in ${}^{11}\text{B}$, *Phys. Rev. Lett.* **124**, 042502 (2020).
- [110] T. Kawabata, Y. Sasamoto, Y. Maeda, S. Sakaguchi, Y. Shimizu, K. Suda, T. Uesaka, M. Fujiwara, H. Hashimoto, K. Hatanaka, K. Kawase, H. Matsubara, K. Nakanishi, Y. Tameshige, A. Tamii, K. Itoh, M. Itoh, H. P. Yoshida, Y. Kanada-En'yo, and M. Uchida, Cluster states in ${}^{13}\text{C}$ and ${}^{11}\text{B}$, *Int. J. Mod. Phys. E* **17**, 2071 (2008).
- [111] A. N. Danilov, T. L. Belyaeva, S. A. Goncharov, A. S. Demyanova, and A. A. Ogloblin, Determination of the radii of some threshold states in light nuclei and observation of neutron halos in the excited states of ${}^{13}\text{C}$ and ${}^9\text{Be}$, *AIP Conf. Proc.* **1224**, 88 (2010).
- [112] A. S. Demyanova, A. A. Ogloblin, T. L. Belyaeva, N. Burtebaev, S. A. Goncharov, Y. B. Gurov, A. N. Danilov, S. V. Dmitriev, Y. G. Sobolev, W. Trzaska, G. P. Tyurin, P. Heikkinen, S. V. Khlebnikov, and R. Julin, Cluster states of ${}^{11}\text{B}$ with abnormally large radii, in *LXII International conference NUCLEUS 2012. Fundamental problems of nuclear physics, atomic power engineering and nuclear technologies*, edited by A. K. Vlasnikov (Russian Academy of Sciences, Moscow, 2012), pp. 25–30.
- [113] M. Freer, N. L. Achouri, C. Angulo, N. I. Ashwood, D. W. Bardayan, S. Brown, W. N. Catford, K. A. Chipps, N. Curtis, P. Demaret, C. Harlin, B. Laurent, J. D. Malcolm, M. Milin, T. Munoz-Britton, N. A. Orr, S. D. Pain, D. Price, R. Raabe, N. Soić *et al.*, Resonances in ${}^{11}\text{C}$ observed in the ${}^4\text{He}({}^7\text{Be}, \alpha){}^7\text{Be}$ and ${}^4\text{He}({}^7\text{Be}, p){}^{10}\text{B}$ reactions, *Phys. Rev. C* **85**, 014304 (2012).

- [114] N. Soić, M. Freer, L. Donadille, N. Clarke, P. Leask, W. Catford, K. Jones, D. Mahboub, B. Fulton, B. Greenhalgh, D. Watson, and D. Weisser, α -decay of excited states in ^{11}C and ^{11}B , *Nucl. Phys. A* **742**, 271 (2004).
- [115] R. J. Charity, S. A. Komarov, L. G. Sobotka, J. Clifford, D. Bazin, A. Gade, J. Lee, S. M. Lukyanov, W. G. Lynch, M. Mocko, S. P. Lobastov, A. M. Rogers, A. Sanetullaev, M. B. Tsang, M. S. Wallace, R. G. T. Zegers, S. Hudan, C. Metelko, M. A. Famiano, A. H. Wuosmaa *et al.*, Investigation of particle-unbound excited states in light nuclei with resonance-decay spectroscopy using a ^{12}Be beam, *Phys. Rev. C* **78**, 054307 (2008).
- [116] S. L. Hausladen, R. O. Lane, and J. E. Monahan, Predictions of differential cross sections for the reactions $^{10}\text{B}(n, \alpha_0)^7\text{Li}$ and $^{10}\text{B}(n, \alpha_1)^7\text{Li}$ (0.48 Mev), *Phys. Rev. C* **5**, 277 (1972).
- [117] M. Wiescher, O. Clarkson, R. J. deBoer, and P. Denisenkov, Nuclear clusters as the first stepping stones for the chemical evolution of the universe, *Eur. Phys. J. A* **57**, 24 (2021).
- [118] N. Curtis, N. I. Ashwood, W. N. Catford, N. M. Clarke, M. Freer, D. Mahboub, C. J. Metelko, S. D. Pain, N. Soić, and D. C. Weisser, $\alpha + \text{Li}$ and $h + \text{Be}$ decay of $^{10,11,12}\text{B}$, *Phys. Rev. C* **72**, 044320 (2005).
- [119] N. Soić, M. Freer, L. Donadille, N. M. Clarke, P. J. Leask, W. N. Catford, K. L. Jones, D. Mahboub, B. R. Fulton, B. J. Greenhalgh, D. L. Watson, and D. C. Weisser, Three-centre cluster structure in ^{11}C and ^{11}B , *J. Phys. G: Nucl. Part. Phys.* **31**, S1701 (2005).
- [120] F. C. Barker, $T = \frac{3}{2}$ levels in $A = 11$ nuclei, *Phys. Rev. C* **69**, 024310 (2004).
- [121] F. C. Barker, Width of $^{11}\text{B}(\frac{1}{2}^+, T = \frac{3}{2})$, *Phys. Rev. C* **76**, 027602 (2007).
- [122] H. T. Fortune, Energy and width of $^{11}\text{B}(1/2^+, T = 3/2)$, *Phys. Rev. C* **74**, 034328 (2006).
- [123] D. L. Auton, Direct reactions on ^{10}Be , *Nucl. Phys. A* **157**, 305 (1970).
- [124] M. Freer, E. Casarejos, L. Achouri, C. Angulo, N. I. Ashwood, N. Curtis, P. Demaret, C. Harlin, B. Laurent, M. Milin, N. A. Orr, D. Price, R. Raabe, N. Soić, and V. A. Ziman, $\alpha : 2n : \alpha$ Molecular Band in ^{10}Be , *Phys. Rev. Lett.* **96**, 042501 (2006).

Correction: The energy for the first excited state in ^{10}Be was incorrectly presented as 3.030 MeV rather than the known value of 3.368 MeV and has been fixed in Table II, the caption to Figure 6, and the first sentence of the fourth paragraph of Sec. IV C. Table V contained some errors and has been fixed: The line starting with 15.02 should be deleted; the dash in the 16.432(10) line should be replaced by $T = (3/2)$.